The Isotopic Composition of Rainfall on a Subtropical Mountainous Island

GIUSEPPE TORRI,[a] ALISON D. NUGENT,[a] AND BRIAN N. POPP[b]

[a] *Department of Atmospheric Sciences, University of Hawai'i at Mānoa, Honolulu, Hawaii*
[b] *Department of Earth Sciences, University of Hawai'i at Mānoa, Honolulu, Hawaii*

(Manuscript received 20 October 2021, in final form 24 November 2022)

ABSTRACT: Tropical islands are simultaneously some of the most biodiverse and vulnerable places on Earth. Water resources help maintain the delicate balance on which the ecosystems and the population of tropical islands rely. Hydrogen and oxygen isotope analyses are a powerful tool in the study of the water cycle on tropical islands, although the scarcity of long-term and high-frequency data makes interpretation challenging. Here, a new dataset is presented based on weekly collection of rainfall H and O isotopic composition on the island of O'ahu, Hawai'i, beginning from July 2019 and still ongoing. The data show considerable differences in isotopic ratios produced by different weather systems, with Kona lows and upper-level lows having the lowest δ^2H and δ^{18}O values, and trade-wind showers the highest. The data also show significant spatial variability, with some sites being characterized by higher isotope ratios than others. The amount effect is not observed consistently at all sites. Deuterium excess shows a marked seasonal cycle, which is attributed to the different origin and history of the air masses that are responsible for rainfall in the winter and summer months. The local meteoric water line and a comparison of this dataset with a long-term historical record illustrate strong interannual variability and the need to establish a long-term precipitation isotope monitoring network for Hawai'i.

SIGNIFICANCE STATEMENT: The isotopic composition of water is often used in the study of island water resources, but the scarcity of high-frequency datasets makes the interpretation of data difficult. The purpose of this study is to investigate the isotopic composition of rainfall on a mountainous island in the subtropics. Based on weekly data collection on O'ahu, Hawai'i, the results improve our understanding of the isotopic composition of rainfall due to different weather systems, like trade-wind showers or cold fronts, as well as its spatial and temporal variability. These results could inform the interpretation of data from other mountainous islands in similar climate zones.

KEYWORDS: Subtropics; Convection; Rainfall; Orographic effects; Isotopic analysis; Interannual variability

1. Introduction

Climate represents an important component of the delicate equilibrium on which the biodiverse ecosystems on tropical islands rest (Veron et al. 2019). As the world begins to deal with the consequences of a changing climate, tropical islands are especially vulnerable to how those changes will manifest at a regional scale (Veron et al. 2019). For example, in Hawai'i more than 99% of the freshwater supply comes from rainfall (Gingerich and Oki 2000). Any disruption to the hydroclimate in the North Pacific region can therefore threaten the ecosystems and the habitability of the islands, which are currently home to more than one million people (USGCRP 2017; U.S. Census Bureau 2020; Murakami et al. 2013; Longman et al. 2021). A better understanding of the climate of tropical islands is needed.

In the study of island climate and ecosystems, analysis of the stable isotopic composition of water is a particularly useful tool. Values of δ^2H and δ^{18}O, or of deuterium excess, can be used to infer where an air parcel originated from, the climatic conditions at the origin, or the microphysical processes that the parcel underwent in its history (Dansgaard 1964; Merlivat and Jouzel 1979; Froehlich et al. 2002; Uemura et al. 2008; Pfahl and Sodemann 2014; Bailey et al. 2015; Galewsky et al. 2016; Guilpart et al. 2017; Otte et al. 2017; Esquivel-Hernández et al. 2019). For example, Uemura et al. (2012) used δ^{18}O and δ^2H values in precipitation on Okinawa to show that the air masses contributing to rainfall on the island have different origins depending on the season. These data were also later used to interpret a 180-yr-long record of δ^{18}O from the island (Uemura et al. 2018). Similar applications to determine moisture transport pathways to islands were also done recently, for example, for the Canary Islands (González et al. 2016; Dahinden et al. 2021), Barbados (Villiger et al. 2022), Iceland (Aemisegger 2018), and Svalbard (Leroy-Dos Santos et al. 2020).

In the context of precipitation isotopic composition, an anticorrelation has been known for a long time between precipitation amount and δ^2H and δ^{18}O values (Dansgaard 1964; Rozanski et al. 1993). This phenomenon, known as the *amount effect*, is particularly pronounced in the tropics, where it has been observed on a variety of time scales (Vimeux et al. 2005; Lee and Fung 2008; Kurita et al. 2009; Scholl et al. 2009; Moerman et al. 2013; Torri et al. 2017), although it does not always appear on an event base (Risi et al. 2008, 2010; Kurita 2013; Conroy et al. 2016a,b; Zwart et al. 2018; He et al. 2018). The amount effect has been widely used, for example, to interpret paleoclimate records (Burns et al. 1998; Wang et al. 2001; Frappier et al. 2002, 2007; Sachs et al. 2009; Vimeux et al. 2009;

Supplemental information related to this paper is available at the Journals Online website: https://doi.org/10.1175/JHM-D-21-0204.s1.

Corresponding author: Giuseppe Torri, gtorri@hawaii.edu

DOI: 10.1175/JHM-D-21-0204.1

Tierney et al. 2010; Beilman et al. 2019; Massa et al. 2021). While a variety of potential explanations have been advanced to explain the amount effect (Lee et al. 2007; Risi et al. 2008; Kurita 2013; Moore et al. 2014), a complete understanding of this phenomenon is yet to be achieved.

Isotopic composition of water can also be used to study islands' hydrology. Comparing δ^2H and δ^{18}O values of water in precipitation with those found in springs and well water, it is possible to determine flow paths and aquifer recharge areas (Bowen et al. 2019). Recent examples of these studies have been conducted in Tahiti (Hildenbrand et al. 2005), Easter Island (Herrera and Custodio 2008), the Cape Verde Islands (Heilweil et al. 2009; Carreira et al. 2010), the island of Rishiri, (Mandal et al. 2011), Madeira (Prada et al. 2016), Galapagos (Martin et al. 2018), and American Samoa (Shuler et al. 2019).

Similar studies to the ones cited above were also conducted in Hawai'i. Friedman and Woodcock (1957) were among the first to measure δ^2H values in rainfall at different elevations on Hawai'i Island. A few decades later, McMurtry et al. (1977) analyzed δ^{18}O and δ^2H values at various locations on Hawai'i Island. More recently, Scholl et al. (1996) sampled precipitation on Hawai'i Island with a 6-month interval from August 1991 to August 1994 and compared δ^{18}O and δ^2H values with those analyzed in groundwater. A 6-month frequency was also used by Scholl et al. (2002), who sampled precipitation on Maui between September 1995 and September 1997. Scholl et al. (2007) collected cloud water and rain at approximately a monthly frequency for a 2-yr period, between August 2001 and August 2003, on East Maui. In recent years, efforts to better understand groundwater resources in West Hawai'i Island have led to a number of investigations in the area: Tillman et al. (2014) sampled precipitation at intervals between 5 and 7 months between 2012 and 2014, Fackrell et al. (2020) sampled at a 6-month frequency for 2 years, and Tachera et al. (2021) collected precipitation between 2017 and 2019 approximately every 3 months. Finally, isotope analysis has also been conducted on precipitation on the island of O'ahu, first by Dores et al. (2020), who sampled rain for 16 months at a 3-month frequency and, more recently, by Booth et al. (2021), who conducted a monthly collection between December 2017 and March 2019, as well as an event-based collection for a period of 5 months.

The longest available record of the isotopic composition of rainfall in Hawai'i was collected with a monthly frequency between 1962 and 1970 as part of the Global Network of Isotopes in Precipitation (GNIP) (IAEA/WMO 2021). However, the lack of reliable satellite data and the scarcity of other weather observations at the time make the interpretation of those isotope data equally challenging. The GNIP dataset also presented another limitation, because all the data were collected in a single location on the windward side of Hawai'i Island, thus potentially introducing biases: for example, the same weather system coming from different directions would likely produce rain with different isotopic compositions thanks to the island orographic effect.

As the examples presented above illustrate, most collections that have taken place in Hawai'i are characterized by sampling frequencies of the order of months, or take place over short periods of time. While month-long frequencies might be adequate to study processes involving groundwater aquifers or to interpret paleorecords (Beilman et al. 2019; Massa et al. 2021), they make interpretation of the amount effect and micrometeorological processes challenging.

Here, a new dataset of δ^2H and δ^{18}O values of rainfall is presented. The data were collected on the island of O'ahu with a weekly or near-weekly frequency over five different sites, two on the windward side and three on the leeward side. The data discussed here span 2 years, from July 2019 until July 2021, although collection is still ongoing. With the data collected throughout this period and with the GNIP dataset, three main questions will be addressed:

- Are there systematic differences between the isotopic composition and deuterium excess in rain collected from different sites?
- Is the amount effect observed at all sites?
- Is there appreciable seasonal and interannual variability in the isotopic composition of rain?

In section 2, all the definitions and the data used for this study are introduced. In section 3, the rainfall isotope dataset is presented. In section 4, the implications of the data are discussed. Finally, conclusions are presented in section 5.

2. Methods

a. Definitions

Throughout this manuscript, three stable water isotopologues are considered: $^1H_2{}^{16}O$, $^1H_2{}^{18}O$, and $^1H^2H^{16}O$. Isotopologues are referred to by the isotope that makes them different from the lighter isotopologue, $^1H_2{}^{16}O$: ^{18}O for $^1H_2{}^{18}O$ and ^2H for $^1H^2H^{16}O$. The isotope ratios of H and O are defined as the concentration of a heavy isotope in a given sample divided by the concentration of the lighter isotope:

$$R_{18_O} \equiv [^{18}O]/[^{16}O] \tag{1}$$

$$R_{2_H} \equiv [^{2}H]/[^{1}H], \tag{2}$$

where the square brackets represent the concentration of an isotope. Isotope abundances are reported relative to international standards defined as

$$\delta X \equiv 1000 \times \left(\frac{R_X}{R_{\mathrm{VSMOW}}} - 1 \right) \tag{3}$$

where R_{VSMOW} is the isotopic ratio of VSMOW, the Vienna Standard Mean Ocean Water standard, and X indicates one of the two heavier isotopes. The unit of measurement for isotopic abundances is permil (‰).

From the isotopic abundances, a second-order parameter, called deuterium excess d can be defined as

$$d \equiv \delta^2\mathrm{H} - 8 \times \delta^{18}\mathrm{O}. \tag{4}$$

The global meteoric water line (GMWL) is an empirical linear relationship between the H and O isotope abundances in water (Craig 1961):

$$\delta^2H = 8 \times \delta^{18}O + 10‰. \quad (5)$$

While the GMWL was originally discovered by considering precipitation samples from all over the world, more regional versions have also been used (Rozanski et al. 1993). These, generally known as local meteoric water lines (LMWLs), represent the same empirical relationship, except that the slope and intercept of the lines can be different from the GMWL. Departures from the GMWL are typically linked to processes, like evaporation, that happen in a given region (Rozanski et al. 1993; Putman et al. 2019).

b. Data

1) The study region

O‘ahu is the third largest island of the Hawaiian Archipelago, a group of islands and islets that extends for thousands of kilometers in the North Pacific region. The surface area of O‘ahu covers approximately 1544 km^2 and its topography has been shaped by two separate shield volcanos: the remnants of the northernmost one constitute the Ko‘olau Range, with a peak at 960 m called Pu‘u Kōnāhuanui; those of the southernmost volcano form the Wai‘anae Range, its highest peak being Mount Ka‘ala with an elevation of 1220 m (State of Hawaii 2004).

The climate of O‘ahu is divided in two main periods: a dry season, which, following other studies (Longman et al. 2021), is here defined as the 6-month window between May and October, and a wet season, which covers the remaining 6 months of the year. A quasi-permanent high pressure center located thousands of kilometers northeast of the island strongly modulates its climate and is responsible for steady trade winds. These have been estimated to blow over the Hawaiian Archipelago 50%–80% of the time during the wet season, and 85%–95% during the dry season (Longman et al. 2021). The orographic lifting provided to the moist airflow by the Ko‘olau and the Wai‘anae ranges on O‘ahu causes cloud condensation and the formation of rain, most of which falls in the vicinity of the mountain ranges (Giambelluca et al. 2013).

Trade-wind showers are not the only weather systems responsible for rainfall on O‘ahu (Kodama and Barnes 1997; Kodama and Businger 1998). During the wet season, a considerable amount of rainfall is often generated in relatively short periods of time by synoptic weather systems, such as cold fronts, upper-tropospheric troughs, and subtropical storms, called Kona lows (Simpson 1952). Tropical cyclones (TCs) also contribute, although these typically occur during the dry season. In a recent study, Longman et al. (2021) analyzed daily rainfall on O‘ahu during the period 1990–2010 and determined that nondisturbance type rainfall caused by trade winds accounted for 70.6% of the total rainfall amount during the 20-yr window, cold fronts for 15.5%, Kona lows for 8.8%, upper-tropospheric lows for 3.6%, and TCs accounted only for 1.6%.

Interannual variability of rainfall in Hawai‘i is linked mainly to two large-scale modes (Chu and Chen 2005). The first is known as El Niño–Southern Oscillation (ENSO) and it happens on temporal scales between 2 and 8 years (Trenberth 1997). Its positive phase, called El Niño, is characterized by an anomalous warming of the central/eastern parts of the tropical Pacific Ocean and a deepening of the Aleutian low. The second phenomenon is known as the Pacific decadal oscillation (PDO) (Mantua et al. 1997), and in its positive phase is characterized by colder sea surface temperatures (SSTs) in the western Pacific Ocean, and warmer SSTs in the central and eastern Pacific Ocean. The PDO is characterized by longer frequencies than ENSO, single phases persisting sometimes over 20 years or longer. In Hawai‘i, positive phases of ENSO tend to lead to lower rainfall amounts compared to the negative phases. Similarly, positive phases of the PDO are typically associated with drier conditions (Chu and Chen 2005).

2) Rainwater collection sites

The rainwater collection network that was built to collect the data presented in this manuscript is made of five sites located on the island of O‘ahu. The locations of the collection sites were chosen to give the network a northeast–southwest orientation. Because this is approximately the direction along which trade winds blow, the network makes it possible to look at the evolution of the isotopic composition of trade-wind showers as they move across the island and over the Ko‘olau Range. Future expansions of the network are planned to include other locations on O‘ahu as well as on other islands in the Hawaiian Archipelago.

On the windward side, the network is composed of two sites, one in the city of Kailua and the other in the residential district of Maunawili. On the leeward side, the site closest to the Ko‘olau Range is at Lyon Arboretum, followed to the south by another site at the Hawai‘i Institute of Geophysics (HIG) on the University of Hawai‘i at Mānoa campus, and, finally, one in Waikīkī. The locations of the sites can be seen in Fig. 1, and a summary of the sites’ names, positions, deployment date, and mean temperature, relative humidity, and annual rainfall (Giambelluca et al. 2013, 2014) is presented in Table 1.

Collections of rainfall at Waikīkī, Lyon Arboretum, and HIG were made through a Palmex Rain Sampler 1, in which water enters through a cylinder measuring 13.5 cm in diameter and is deposited in a 3-L HDPE plastic bottle (Gröning et al. 2012). At Maunawili, collections were made through a Palmex Rain Sampler 2, which differs from the others only for its larger size and for the volume of the HDPE plastic bottles used (either 6 or 10 L instead of 3 L). In Kailua, rainfall was collected using a 1-L separatory funnel fitted with a 13.0-cm diameter funnel and filled with approximately 50 mL of heavy mineral oil to prevent evaporation.

Restrictions put in place because of the COVID-19 pandemic—as well as concerns about our own safety—made some collections particularly challenging: Lyon Arboretum was closed to the public for several weeks in March and April 2020. Heavy precipitation that fell during those weeks caused the rain sampler to overflow, and the data are considered inaccurate. Data collection at Waikīkī was discontinued in March 2020 due to challenges imposed by the pandemic and because the scarcity of rainfall in that area made weekly sampling challenging.

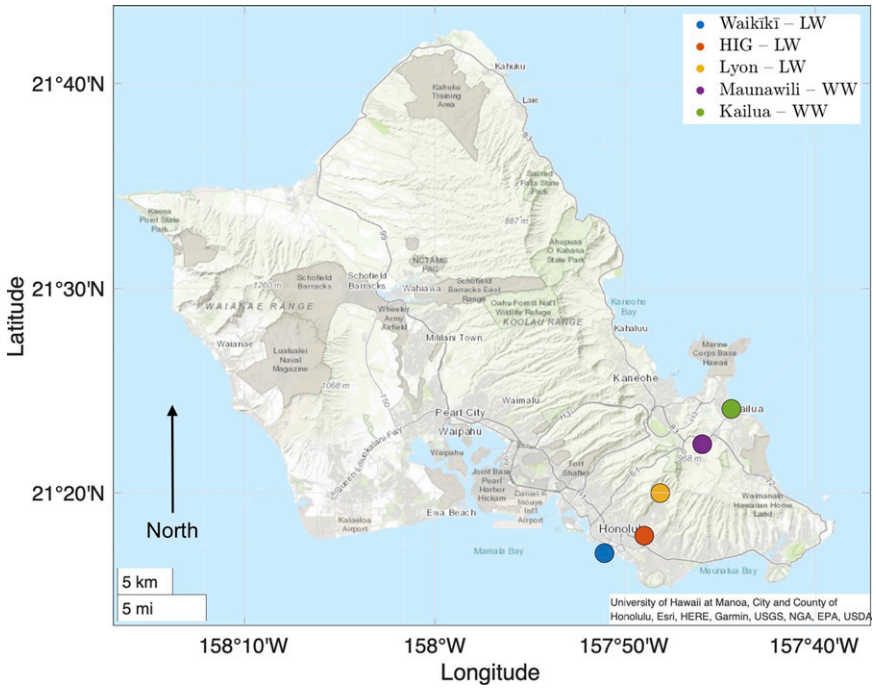

FIG. 1. Map of O'ahu with the five rainfall collection sites which span from the windward to the leeward side of the island, across the Ko'olau Mountain range, marked by colored circles: Kailua (green), Maunawili (purple), Lyon Arboretum (yellow), HIG (orange), and Waikīkī (blue).

In addition to the collection in April 2020, there were a couple of other times when debris was found in the funnel of the rain sampler, which caused it to overflow. In turn, this could have affected the isotopic composition of the rainwater: for example, the partial obstruction could have slowed down the flow of the water into the funnel, thus exposing it to additional evaporation when still in the funnel. While still reported in the figures in this manuscript, data from these collections are marked with crosses. One sample collected from Maunawili on 17 July 2020 was excluded from the analysis, as it was characterized by a negative deuterium excess value approximately 10σ below the weighted mean from that site. The sample covered a week characterized by very low precipitation (0.20 mm day^{-1} on average), and its low deuterium excess value was attributed to postcollection evaporation.

Because the data was collected over 2 years, data from the Global Network of Isotopes in Precipitation (GNIP) are also considered to investigate interannual variability of rainfall isotopic composition in Hawai'i. GNIP is a network that was created in 1957 by the International Atomic Energy Agency and the World Meteorological Organization (IAEA/WMO 2021). Sites were deployed in multiple locations throughout the

TABLE 1. Summary of location and climate information about the rainfall collection sites deployed on O'ahu and of the GNIP site in Hilo from where data used in this manuscript were collected.

Site	Latitude	Longitude	Elevation (m)	Deployment	Samples	Temperature (°C)	RH (%)	Annual rainfall (mm)
Kailua	21°24′60″N	157°44′25″W	8.5	6 Jul 2019–current	110	23.61°C	69.91	987.7
Maunawili	21°22′22″N	157°45′57″W	27.4	5 Oct 2019–current	68	23.35°C	70.47	1405.0
Lyon Arb.	21°19′59″N	157°48′09″W	132.3	25 Jul 2019–current	104	21.54°C	75.59	3931.8
HIG	21°17′54″N	157°48′60″W	40.8	28 Sep 2019–current	81	23.47°C	70.57	931.3
Waikīkī	21°17′02″N	157°50′29″W	2	4 Oct 2019–14 Mar 2020	13	23.75°C	69.91	653.2
Hilo (GNIP)	19°43′12″N	155°4′12″W	9	1 Feb 1962–1 Oct 1969	87	22.75°C	69.98	3428.4

entire world, and collections were typically done with a monthly frequency. In Hawai'i, only one GNIP site was deployed in Hilo, a town on the windward side of Hawai'i Island, and data were collected monthly from 1962 until 1970.

3) ISOTOPE ANALYSIS

Hydrogen and oxygen isotopic composition of rainwater was determined using a cavity ring-down spectroscopy machine—a L2130-I, Picarro—equipped with a high-precision vaporizer (V1102-I, Picarro, Inc., Santa Clara, California) and autosampler (HTC PAL, Leap Technologies, Carrboro, North Carolina) with Chem-Correct acquisition software that monitors for interference of isotopologues of water by organic compounds (Gupta et al. 2009). All measurements were performed in the nitrogen carrier mode, using ultra-high-purity nitrogen (<10 ppm H_2O, >99.99% N_2; Matheson, Irving, Texas) using eight 1.2-μL injections.

Typically, results from the first 3–4 injections were discarded depending on the degree of carryover from the previous analysis as determined by the stability of the measured $\delta^{18}O$ and $\delta^{2}H$ values during manual inspection of the results for each sample. Measured $\delta^{18}O$ and $\delta^{2}H$ values were normalized to VSMOW using results of analysis of three laboratory reference materials that were extensively calibrated with NIST reference materials and had $\delta^{2}H$ and $\delta^{18}O$ values that bracketed the values of all samples (Table S1 in the online supplemental material). These laboratory reference waters were analyzed so that they bookended every 8 to 14 unknowns. Within every 8–14 samples analyzed, a fourth reference water of known isotopic composition (EVIAN) was analyzed as an unknown. Based on repeated measurements ($n = 50$) of this internal laboratory reference water, the precision for this method was determined to be less than 0.05‰ for $\delta^{18}O$ values and 0.5‰ for $\delta^{2}H$ values. Our ability to replicate the $\delta^{18}O$ and $\delta^{2}H$ values of EVIAN for these same analyses reported as the difference in measured and accepted $\delta^{18}O$ and $\delta^{2}H$ values (Table S2), a measure of accuracy of this technique, averaged 0.01‰ and 0.2‰, respectively.

The statistical significance of the differences in the values of $\delta^{18}O$, $\delta^{2}H$, and deuterium excess from different sites is assessed using a two-sample weighted t test with a 95% confidence level (Goldberg et al. 2005). When determining the LMWL, a model II linear regression is used. The regression is conducted using the function "gmregress" on MATLAB, which computes the slope as a geometric mean of the linear regressions coefficients after having removed the mean of the variables and reduced their standard deviation to 1 (Ricker 1973; Trujillo-Ortiz 2022). The correlation between $\delta^{18}O$ values and rain rates is tested using Spearman's rank correlation coefficient, which is particularly useful when the relationship between two variables is not necessarily linear.

4) WEATHER AND CLIMATE DATA

To facilitate the interpretation of isotope data, particularly to distinguish periods characterized by large-scale disturbances from those dominated by trade-wind flow, Monthly Precipitation Summaries from the National Weather Service for the entire collection period were obtained (K. Kodama 2022, personal communication). The information from the summaries was synthesized by defining four categories of possible disturbances (Kodama and Businger 1998): tropical cyclone (TC), upper-level low (UL), cold front (CF), and Kona low (KL). For every site, if at least one disturbance was noted in the precipitation summaries with a date during a sampling period, the precipitation sample was manually flagged as "disturbed." If no disturbance was noted, then the samples from the sites were flagged as "nondisturbed." While the phenomenology of weather disturbances in Hawai'i is significantly richer than four rigid categories (Longman et al. 2021), this classification is an adequate starting point to distinguish rain samples that likely received significant contributions from synoptic systems from those that were only generated by trade winds.

To aid in the interpretation of results from HIG (greater $\delta^{18}O$ and lower deuterium excess values), weather data from this site are considered and compared with data from Lyon Arboretum. Similarly detailed weather data were not available for the other sites. Hourly rainfall data from HIG were collected using a Campbell Scientific TE525WS Texas Electronics Tipping Gauge (8-in. orifice), whereas hourly relative humidity data were collected using a Campbell Scientific EE181-L air temperature and relative humidity sensor. The former has an accuracy of ±1% at rates up to 1 in. h^{-1}, whereas the latter has an accuracy of ±1.3% for the temperatures and relative humidities typically found on O'ahu. The data cover a time interval between 16 October 2019 and 27 August 2021.

Rainfall and relative humidity data from Lyon Arboretum were collected at a 15-min frequency using a CR3000 Campbell Scientific datalogger and associated sensors (HUMICAP 180R sensor for relative humidity). In order for rainfall data to be directly comparable with those from HIG, they were converted into hourly with a simple accumulation sum. For typical conditions at Lyon Arboretum, the accuracy of the humidity sensor is ±1%, whereas for the rain gauge it is ±1% up to 2 in. h^{-1} of rain. Both rainfall and relative humidity data at Lyon Arboretum cover a period from 23 February 2018 to 26 April 2021. When comparing datasets from HIG and Lyon Arboretum, only the data during a time period for which the two datasets overlap (16 October 2019–26 April 2021) are considered. Finally, to connect the interannual variability of the $\delta^{18}O$ values at Hilo with the large-scale conditions, the latter are compared with monthly SST values from the NOAA Extended Reconstructed Sea Surface Temperature V5 (ERSST) dataset (Huang et al. 2017).

5) HYSPLIT

To diagnose the origin of air parcels bringing rain to O'ahu, the NOAA Air Resources Laboratory's Hybrid Single Particle Lagrangian Integrated Trajectory (HYSPLIT) model, version 5.1.0 for Linux, was used (Draxler and Hess 1998; Stein et al. 2015). The model uses meteorological data to compute the forward/backward transport and dispersion of a tracer or of a number of trajectories. It is extensively used in the study of atmospheric processes, with applications including transport of pollutants, allergens, or volcanic ash (Stein et al. 2015).

Following similar approaches to previous studies (e.g., Sodemann et al. 2008; Uemura et al. 2008; Barras and Simmonds 2009; Guan et al. 2013; Aemisegger et al. 2014; Permana et al. 2016; Sánchez-Murillo et al. 2017; Martin et al. 2018; He et al. 2018; Esquivel-Hernández et al. 2019; Papritz et al. 2021; Villiger et al. 2022; Dahinden et al. 2021), HYSPLIT was used to interpret the deuterium excess data. First, a temporal window of 24 months, from 1 July 2019 until 30 June 2021, was selected. This choice was made in order to maximize the overlap with the collected isotope data and also to maintain a symmetry between the number of wet- and dry-season months considered. Then, for each day during the time window, 27 trajectories were initialized at 0000 UTC at a point with the same latitude–longitude coordinates as Lyon Arboretum at an altitude of 500 m, and their positions were integrated backward in time for 5 days. The integration was conducted using meteorological data from ERA5 reanalysis (Hersbach et al. 2019). The 27 trajectories are initialized in a $3 \times 3 \times 3$ cube, each member of this ensemble being calculated by offsetting the meteorological data by one meteorological grid point in the horizontal directions and 0.01 sigma units in the vertical.

The choice of initializing the trajectories at 500 m was made to ensure that the calculation would capture air parcels that are most likely to contribute to rainfall on O'ahu: because of the trade-wind inversion that persists at an altitude of approximately 2–2.5 km for most of the year (Cao et al. 2007; Longman et al. 2015), parcels in the free troposphere are unlikely to contribute often, except during precipitation from synoptic systems. Sensitivity tests were conducted by initializing trajectories at 1000 m and at 1500 m, but the conclusions reached were qualitatively the same (see Figs. S1 and S2). Sensitivity tests were also conducted by only considering trajectories initialized in periods when rainfall was collected at Lyon Arboretum, but no qualitative difference was noticed (not shown).

3. Results

a. Rainfall

For the collection period discussed here, the time series of rainfall rates observed at each site are presented in Fig. 2a. The rates are computed by dividing the amount of water collected at each sampling period by the number of days over which the collection took place (Giambelluca et al. 2013). As expected, the figure shows that the highest rain rates were recorded during the wet season, between the months of October and April. The symbols at the top of Fig. 2a represent the main weather disturbances that were noted in the Precipitation Summaries during the collection period, and they suggest that peaks in rain rates during the wet season are primarily due to upper-level lows and cold fronts. Kona lows were also observed, although they were less frequent than the other categories.

The dry season tends to be characterized by lower rain rates, mostly due to trade wind showers. Occasionally, TCs and tropical storms (TSs) can affect the Hawaiian Islands during the dry season. During the collection period, four TC/TS events were recorded. First, on 8 July 2019, the remnants of TC Barbara passed south of the islands and brought rainfall to the islands, especially on the windward side. Following that, the remnants of TC Erik and Flossie also affected Hawai'i on 12 and 16 July 2019, respectively. Although, as will be seen later, rainfall from these three systems had a different isotopic composition compared to trade-wind showers, the rainfall rates were not significantly higher. The following year, TC Douglas passed remarkably close to the Hawaiian Islands around 25 July 2020. Enhanced rainfall rates by Douglas can be seen in Fig. 2a, especially for the Kailua and the Lyon Arboretum sites.

Another important feature shown by Fig. 2a is that significantly more rainfall is often collected at Lyon Arboretum than all the other sites. For example, as can be inferred from Fig. 3, the median rain at Lyon Arboretum is 8.03 mm day^{-1}, whereas at HIG, only 4 km downwind, it is 1.35 mm day^{-1}, which is comparable to the median rate recorded at the other sites. Considering the location of the Lyon Arboretum rain collector, this can easily be explained as due to orographic enhancement provided by the Ko'olau mountains.

b. Rainfall H and O isotopic composition

The time series of δ^{18}O and δ^{2}H values for the five deployed sites are shown in Figs. 2b and 2c, respectively. The lowest values of δ^{18}O and δ^{2}H were recorded in March 2020 during a Kona low (δ^{2}H $\sim -63.6‰$ at the Kailua site) and in March 2021 when a particularly strong upper-level low affected the island. A Kona low was also observed in October 2021, but it did not produce particularly low δ^{18}O and δ^{2}H values. Rainfall from TCs, or their remnants, also appear to have low δ^{2}H and δ^{18}O values (δ^{2}H $\sim -32.0‰$), although not as low as Kona lows and upper-level lows. A low pressure system to the north of the islands on 10–11 October 2019 led to the advection of moist flow from the southeast, which ultimately resulted in a series of thunderstorms that produced very low δ^{2}H values ($\sim -52.6‰$ at the Waikīkī site)

To gain a more quantitative understanding of the isotopic composition of rainfall collected, and in order to compare the data with similar datasets on O'ahu, a summary of the volume-weighted averages of isotopic abundances for each site is shown in Fig. 4. The numerical values are reported in Table S2.

A weighted two-sample t test conducted on the results suggests that the differences between the total weighted means of δ^{2}H and δ^{18}O values collected at Lyon and those from other sites are statistically significant at 95% confidence level. This holds true also when considering only the wet season, except for the differences between the weighted means at Lyon and Waikīkī sites, whereas most differences between dry-season mean values are not statistically significant. For completeness, Tables S3 and S4 in the supplemental material show the p values determined by comparing δ^{18}O and δ^{2}H values between different sites and for different sampling methods (total, wet season, dry season, disturbed, nondisturbed).

Another way of subsampling the collected data is to distinguish between the isotopic composition of precipitation caused by synoptic systems, such as cold fronts and upper-level lows, and that by trade-wind showers. Figures 4e and 4f show the average δ^{18}O and δ^{2}H values during disturbed (green) and

FIG. 2. Time series of weekly (a) rain rates, (b) δ^{18}O, (c) δ^{2}H, and (d) deuterium excess for the five rainfall collection sites from July 2019 to September 2021. Rain rates are determined as the total accumulated rain for each collection period divided by the time since the previous collection. Lines of different colors indicate data from different sites, with LW indicating a leeward and WW a windward site, and symbols at the top are used to denote the type of weather system that affected the Hawaiian Archipelago during the collection period (see text for more details).

nondisturbed sampling periods (purple) as defined in section 2. A two-sample weighted t test suggests that most of the differences between the various sites of the weighted means of δ^{18}O and δ^{2}H values measured during nondisturbed periods are not statistically significant, the only exception being δ^{18}O mean values at Lyon Arboretum and Kailua, which appear different at 95% confidence level. On the other hand, mean values during disturbed weeks show some significant differences (see Tables S2 and S3).

To gain a better understanding of the differences between precipitation collected at HIG and at other nearby locations, the daily accumulated rainfall at HIG is matched with the daily accumulated rainfall at Lyon Arboretum, and the result is presented in Fig. 5a. Figure 5b shows the cumulative distribution function of daily accumulated rainfall at HIG for days when more than 0.5 mm of rain was collected at Lyon Arboretum. The curves show that, for 41.5% of those days during the wet season and for 68.0% during the dry season, no rainfall was collected at HIG in spite of some being recorded at Lyon Arboretum. The numbers increase when attention is restricted to days with small amounts of precipitation at Lyon Arboretum that do not exceed 5 mm (53.3% during the wet season and 72.6% during the dry season; not shown). This result emphasizes the strong gradient in rainfall between these two collection sites, further discussed in section 4.

c. *The amount effect*

Figures 6a–e show δ^{18}O values of rainfall as a function of the average rain rate during each collection period (δ^{2}H values look very similar but are not shown). Data in different panels

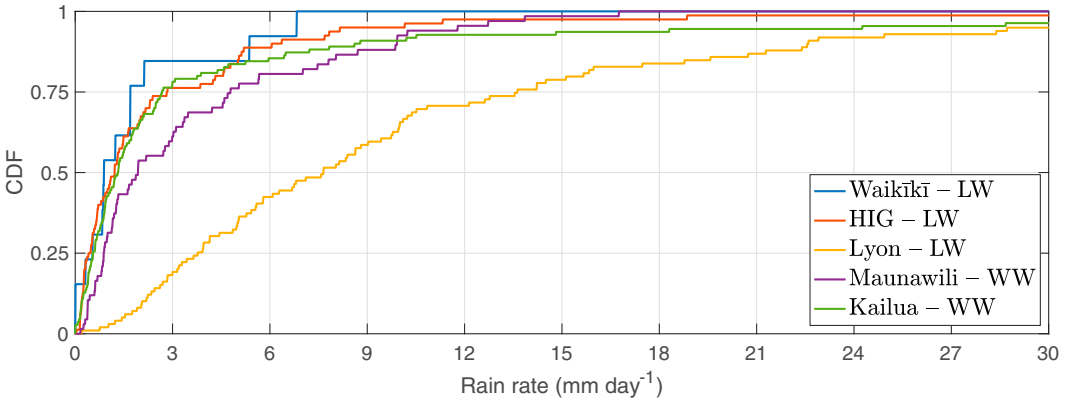

FIG. 3. Cumulative distribution functions of rain rates for the various sites.

were sampled using different criteria (e.g., dry season only, wet season only, etc.). Because Lyon Arboretum is characterized by larger rain rates than any other site, and given that the sites have similar distribution functions of rain rates (Fig. 3), the data are presented as a function of rain rate percentiles.

Overall, rainfall appears to have a remarkably consistent isotopic composition. On the one hand, as Fig. 3 illustrates, the bottom 75 percentiles correspond to relatively small rain rates, especially for leeward sites. On the other hand, during the dry season (Fig. 6c) or for nondisturbed sampling periods (Fig. 6e), even samples at top percentiles do not have particularly low δ^{18}O values.

To quantify the "strength" of the amount effect, Fig. 6f shows the Spearman correlation coefficients computed between δ^{18}O values and rain rates for different sites and for all the different sampling types shown in the other panels. Given that higher rain rates should have lower ^{18}O/^{16}O ratios with the amount effect, one would expect negative coefficients for all sites. The values of the coefficients for the sites at Kailua and HIG are relatively similar for all sampling types, but the sites at Maunawili and Lyon Arboretum show greater variability. In the case of Lyon Arboretum, the lowest coefficient (−0.52) is computed for the wet season and the highest (0.04) for the nondisturbed samples. A p value test on the coefficients suggests that all are significantly different from 0, with the exception of some values recorded at Waikīkī and those with values greater than −0.2: the dry season coefficients for Lyon Arboretum and Maunawili and the nondisturbed Lyon Arboretum value. A summary of the values of all the coefficients can be found in Table S6.

d. *Deuterium excess*

The time series of deuterium excess derived from Eq. (4) for the five sites is presented in Fig. 2d. The figure shows two

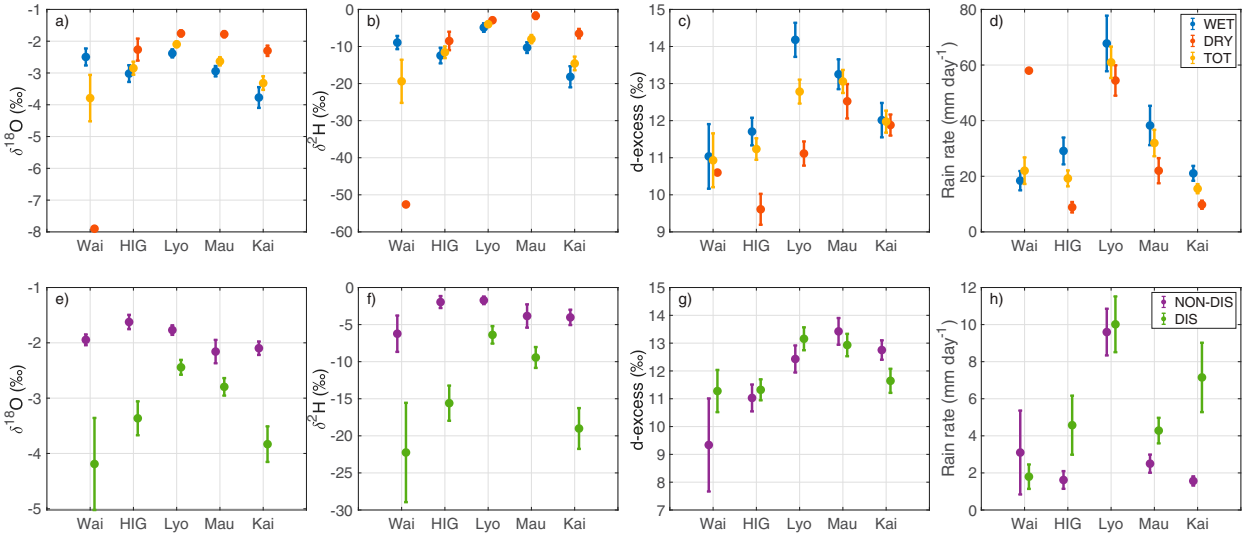

FIG. 4. Volume-weighted averages and their standard errors of (a) δ^{18}O, (b) δ^{2}H, (c) deuterium excess, and (d) rain rate over the entire collection period (yellow, TOT) and over the dry (red, DRY) and wet seasons only (blue, WET). (e)–(h) As in (a)–(d), but for data divided between disturbed (green, DIS) and nondisturbed (purple, NON-DIS) sampling periods. Sites are listed from the most leeward to the most windward from left to right. For the Waikīkī site, the average value for the dry season appears without a standard error because only one data point was available for that sampling period.

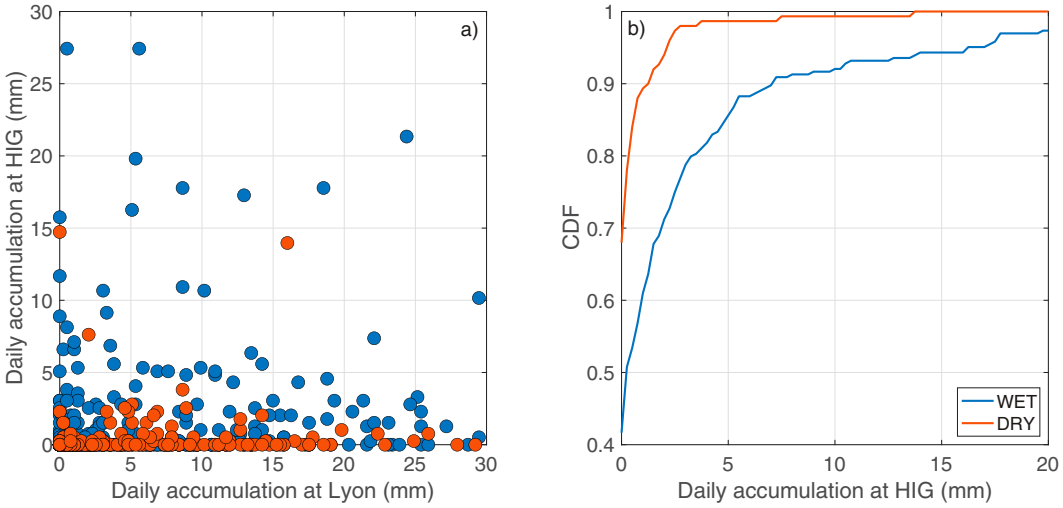

FIG. 5. (a) Daily accumulated rainfall at HIG shown as a function of rainfall accumulated at Lyon Arboretum for the same day. (b) Cumulative distribution function of daily accumulated rainfall at HIG for days during the wet (blue) and dry (red) season when more than 0.5 mm of rain was collected at Lyon Arboretum.

interesting features. The first is the apparent seasonal cycle, with higher deuterium excess during the wet season and lower values during the dry season, and a difference between the two of approximately 5‰. This phenomenon has been observed both on a global scale (Araguás-Araguás et al. 2000; Pfahl and Sodemann 2014) and at a regional level in other locations (Delmotte et al. 2000; Yoshimura and Ichiyanagi 2009; Guan et al. 2013; Kopec et al. 2019). The other interesting feature of Fig. 2d is that, particularly during the dry season, the HIG site has consistently lower deuterium excess compared to other sites.

Because deuterium excess has been shown to be sensitive to relative humidity and SST at the moisture source (Merlivat and Jouzel 1979; Uemura et al. 2008; Pfahl and Sodemann 2014), changes in the environmental conditions at the source, or the presence of different sources, are typically used to explain seasonal changes to deuterium excess values. A more quantitative comparison of the deuterium excess values measured at the five sites are presented in Fig. 4c, which represent the volume-weighted averages for the entire collection period, for the wet season and for the dry season only, and in Fig. 4g for the disturbed and nondisturbed samples.

e. *The Local Meteoric Water Line*

The black line in Fig. 7a represents the LMWL for O‘ahu determined using a linear regression based on all the data collected (shown in colored crosses). While most data points seem to align relatively well with the LMWL, data at the extremes—either very low or very high values of δ^2H and δ^{18}O—appear to lie under the LMWL, potentially an indication of subcloud rain evaporation. The slope and the intercept of the LMWL, as well as the R^2 value, are shown by the leftmost blue and red points in Fig. 7b.

As a way to test the sensitivity of the LMWL to the geography of the network and the temporal window over which the collection is conducted, Fig. 7b also reports results from a simple experiment. Starting from the left, the second and third pairs of dots in each panel of the figure represent the slopes and the intercepts of the LMWL obtained by considering sites in the windward (Kailua and Maunawili) and those on the leeward (Lyon Arboretum, HIG, and Waikīkī) side of the island, respectively. The fourth and fifth pairs of dots from the left of each panel contain results from regressions conducted using all data from 1 July 2019 to 30 June 2020 and from 1 July 2020 to 30 June 2021, respectively. The other dots represent the slopes and the intercepts determined in other studies conducted in Hawai‘i. The bars represent 95% confidence intervals. The numerical values of all the slopes and intercepts are reported in Table S7.

The results show considerable variability, which naturally raises the question of what spatial and temporal scales must be taken into consideration in order to determine a LMWL that is representative of O‘ahu and, more generally, the Hawaiian Archipelago.

f. *Trajectory analysis*

To provide a better understanding of the seasonal variations of deuterium excess values observed in Fig. 2d, HYSPLIT trajectories are examined. As an example of the different kinds of paths followed by trajectories reaching O‘ahu, Fig. 8a shows all the trajectories that reached the island in the period from 2 to 5 March 2021; Fig. 8b the trajectories between 10 and 17 July 2020. These two particular periods were chosen because they represented two different situations from the perspective of deuterium excess values: as Fig. 2 suggests, the former period coincides with a time when some of the highest values were recorded, whereas the opposite holds for the latter.

Figure 8 suggests that, during the wet season, trajectories might come from more remote regions and greater altitudes than during the dry season. While this is intended only as an

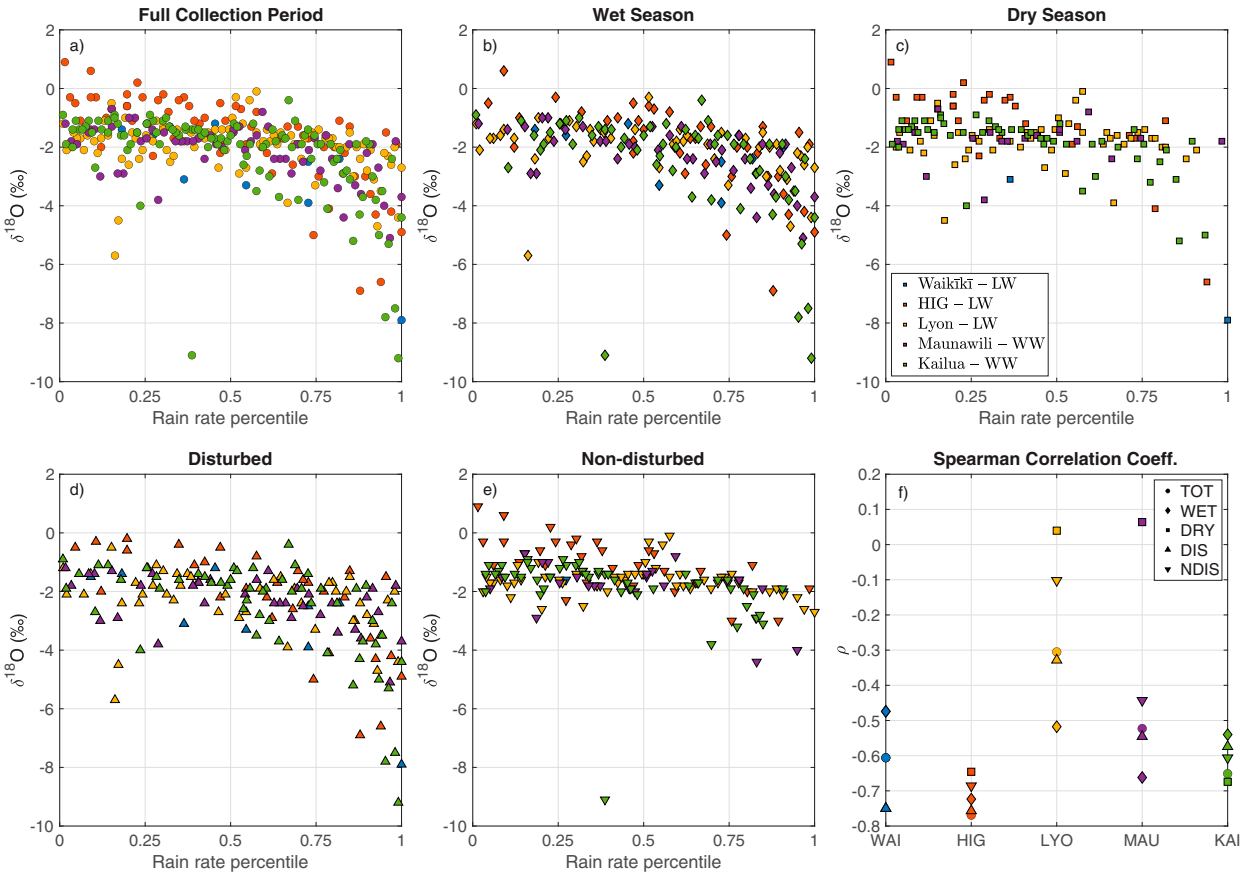

FIG. 6. δ^{18}O values as a function of rain rate percentile for each site shown for the (a) entire collection period, (b) only considering wet-season rainfall, (c) only considering dry-season rain, (d) disturbed periods, and (e) nondisturbed periods. (f) Summary of Spearman correlation coefficients computed between δ^{18}O values and rain rates for each site and for the different types of sampling.

illustrative example, plots for other collection periods with similar deuterium excess values confirm the results (not shown).

The altitude of the trajectories as they approach O'ahu in different seasons is then analyzed. Each trajectory is examined and the time when it last descended below an altitude of 2.2 km is recorded. For simplicity, this quantity will be referred to as *time of last entry*. The threshold of 2.2 km was chosen as representative of the boundary layer height in Hawai'i (Longman et al. 2015), inside of which air parcels are strongly affected by surface conditions. If a trajectory was never above the boundary layer, its time of last entry is set to infinity.

In Fig. 8c, the cumulative distribution functions of times of last entry are shown: the yellow curve refers to all the trajectories, whereas the red and the blue curve are for the trajectories that reach O'ahu in the dry and wet season, respectively. Sensitivity tests were conducted where the height of the boundary layer was varied to 2 and 3 km, and no qualitative changes were noticed (not shown).

Trajectories are then matched with physical variables from ERA5 in order to estimate the atmospheric conditions that air parcels encountered while approaching O'ahu. The values of relative humidity and potential temperature for each trajectory are recorded as a function of height and time before the trajectory's arrival on O'ahu. Then, average values are computed for the dry season and for the wet season. The differences between these two averages are shown in Figs. 9a and 9b. A similar method was also followed for SST, by matching the horizontal position with the values at the surface. The average SST for the entire period as a function of time before arrival is shown by the yellow curve in Fig. 9c, whereas the averages for the dry and wet period are shown by the red and blue curve, respectively. Sensitivity experiments were conducted where the initial height of the trajectories was varied to 1000 and 1500 m. The results are shown in Figs. S1 and S2 and are qualitatively the same as those shown in Fig. 9.

g. *Interannual variability*

To gain a better appreciation for the intraseasonal variability of the rainfall isotopic composition in Hawai'i, Figs. 10a and 10b represent the isotopic abundances recorded at the GNIP site of Hilo during the wet and the dry seasons, respectively. The plots show that, while rain during the dry season tends to have a more consistent isotopic composition throughout the years of data collection, rain during the wet season

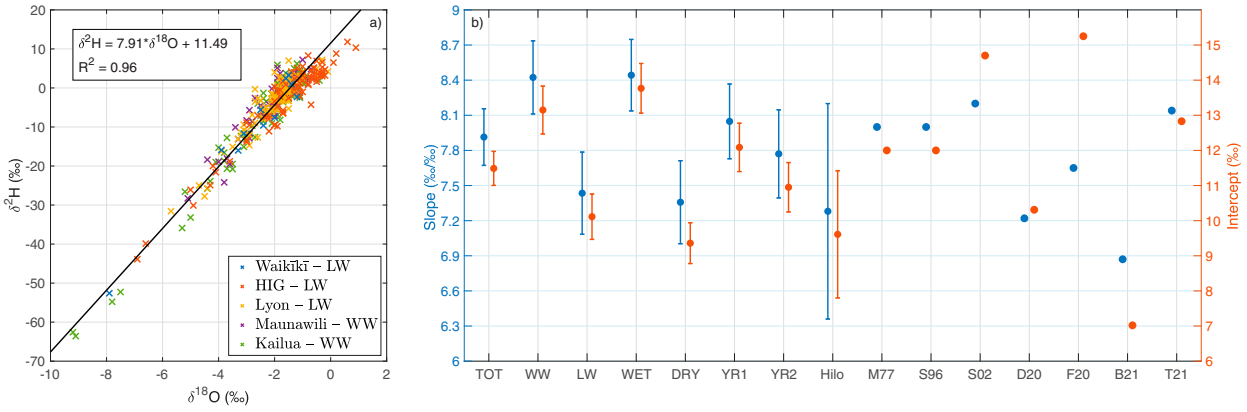

FIG. 7. (a) LMWL (black line) diagnosed from a linear regression of all data from the five sites (colored crosses) over the entire collection period. The slope and the intercept of the linear regression, as well as the R^2 are reported in the top-left corner. (b) Values of the slope (blue) and the intercept (red) computed with a model II regression over all the data (TOT), only windward sites (WW), only leeward sites (LW), data only from the wet season (WET), dry season (DRY), first year of collection (YR1), second year of collection (YR2), the data from GNIP Hilo (Hilo), McMurtry et al. (1977) (M77), Scholl et al. (1996) (S96), Scholl et al. (2002) (S02), Dores et al. (2020) (D20), Fackrell et al. (2020) (F20), Booth et al. (2021) (B21), and Tachera et al. (2021) (T21).

shows greater variability: although with some exceptions, the data from latter half of the collection tend to have lower $\delta^{18}O$ and δ^2H values than those in the first part. Data from Hilo are then separated by year and an interpolation line is computed for each year. The slopes and the intercepts, as well as the 95% confidence intervals, are shown in Fig. 10c.

The reasons for the observed interannual variability and for the difference between the behavior in the wet and the dry season are further investigated by examining the correlation between SST and rainfall isotopic composition in Hilo. For each grid box in the ERSST dataset, a linear regression is conducted between the normalized $\delta^{18}O$ values at Hilo and the time series of SST anomalies at the grid box considered. The $\delta^{18}O$ values are normalized by first subtracting the volume-weighted mean and then dividing the results by the volume-weighted standard deviation. The coefficients of the linear regression are represented in Fig. 11.

While the correlation between normalized $\delta^{18}O$ values of SST anomalies is significant with 95% confidence in relatively small areas (enclosed by the dotted curves), there appears to be a positive correlation between the two variables in the equatorial and subtropical west Pacific, and negative correlations in the subtropical central and eastern Pacific. Figures S3 and S4 show the coefficients obtained only considering the wet and the dry seasons, respectively, and suggest that the correlation between $\delta^{18}O$ values and SST anomalies is much weaker during the dry season than the wet season.

4. Discussion

Although the hydrogen and oxygen isotopic composition of water has been used in many different areas within the study of climate, an incomplete understanding of how various atmospheric processes affect the isotopic composition of precipitation contributes to making the interpretation of records difficult. While numerical models can be a key to progress, the relative lack of long-term high-frequency time series of δ^2H and $\delta^{18}O$ values can be a hindrance to this progress. This study contributes to the current debate by introducing a new dataset of rainfall isotopic composition on the island of O'ahu.

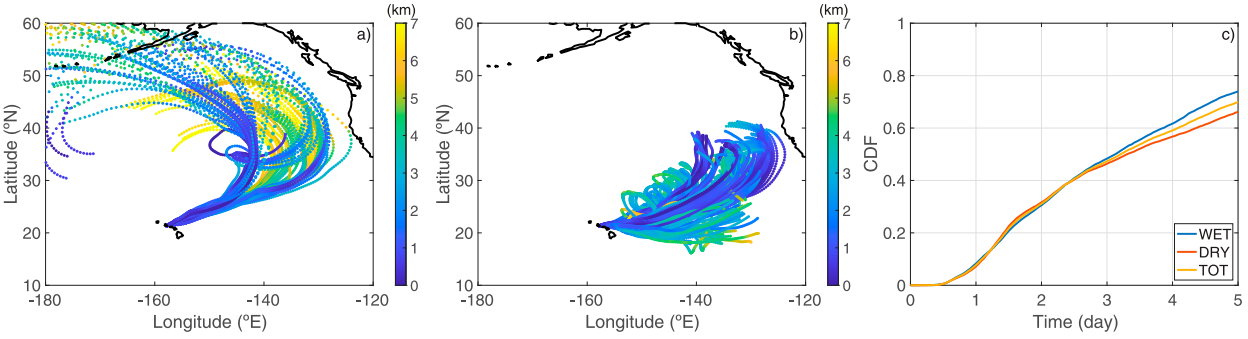

FIG. 8. Examples of 5-day trajectories that reach O'ahu in the period (a) 2–5 Mar 2021 and (b) 10–17 Jul 2020, when high and low deuterium excess values were found in (a) and (b), respectively. (c) Cumulative distribution function of time of last entry for trajectories over the entire collection period (yellow), dry season (red), and wet season (blue).

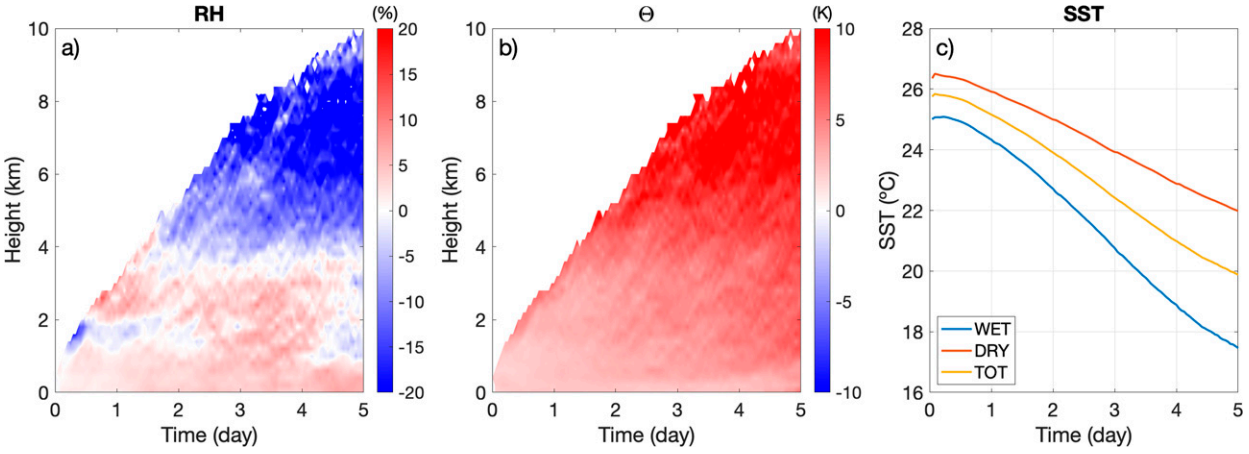

FIG. 9. Differences between the dry season and the wet season values of (a) relative humidity and (b) potential temperature experienced by the trajectories reaching O'ahu. (c) Values of SST in the ocean below the trajectories for the wet season (blue), the dry season (red), and for the entire collection period (yellow).

Compared with other studies that have taken place in Hawai'i (e.g., Friedman and Woodcock 1957; McMurtry et al. 1977; Scholl et al. 1996, 2002, 2007; Tillman et al. 2014; Fackrell and Glenn 2014; Kelly and Glenn 2015; Fackrell et al. 2020; Tachera et al. 2021; Booth et al. 2021), one advantage of the data discussed here is that the increased temporal resolution gives a clearer picture of the isotopic composition of rainfall due to different types of synoptic systems or weather disturbances. Recently, Booth et al. (2021) were able to sample data on an event base, although only for a few months. While frequent collections at various sites require significant efforts, the insights gained from the results presented here and those of Booth et al. (2021) will hopefully inspire more on this front.

a. Rainfall isotopic composition

In almost all sites, rainfall appears to be characterized by lower values of δ^2H and δ^{18}O during the wet season than the dry season, something that had been noticed by collections on the other islands as well (Scholl et al. 1996, 2002, 2007; Tillman et al. 2014; Kelly and Glenn 2015; Fackrell et al. 2020; Tachera et al. 2021; Booth et al. 2021). The only exception is at Waikīkī, although only one data point was collected in the dry season at that site. Such low values at Waikīkī (δ^{18}O = −7.9‰ and δ^2H = −52.6‰) were attributed to a low pressure system that caused heavy rainfall and a series of thunderstorms on the island. In general, given its location, the site at Waikīkī was characterized by little rainfall (Giambelluca et al. 2013), and most orographically generated trade-wind showers did not bring much precipitation there.

Significant differences were also observed between samples where synoptic systems had contributed (disturbed) and those that were mostly dominated by trade-wind flow (nondisturbed). Similar results were also found by other investigators in Hawai'i, who showed that large-scale systems were associated with lower δ^2H and δ^{18}O values than trade-wind showers (Dores et al. 2020; Tachera et al. 2021; Booth et al. 2021). These differences were also recently invoked to interpret paleorecords from peatlands on Moloka'i (Beilman et al. 2019) and O'ahu (Massa et al. 2021) over the last 12 and 45 ka before present (BP), respectively: relatively low δ^2H values

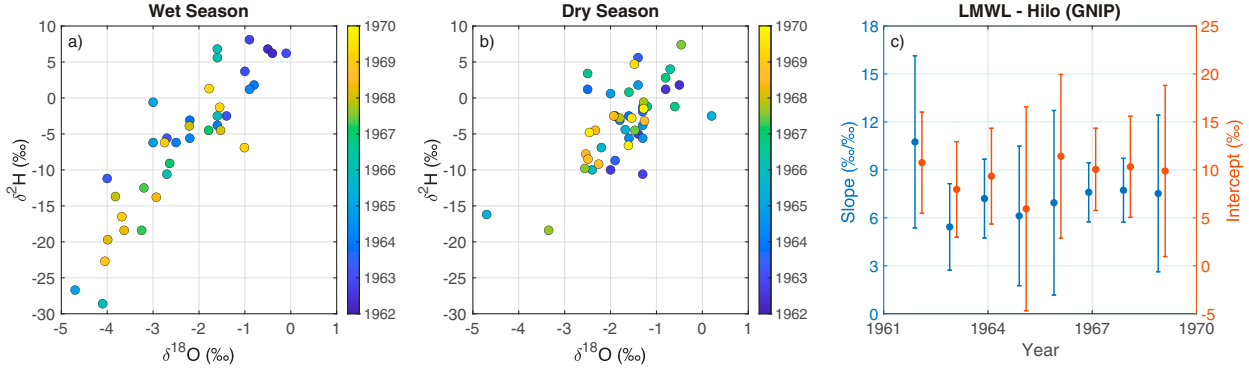

FIG. 10. δ^2H values for the (a) wet season and the (b) dry season shown as a function of δ^{18}O values for the GNIP data at Hilo. Colors reflect the year and the month when data were collected. (c) Slopes (blue) and intercepts (red) and relative errors of LMWL computed for each year from data at Hilo.

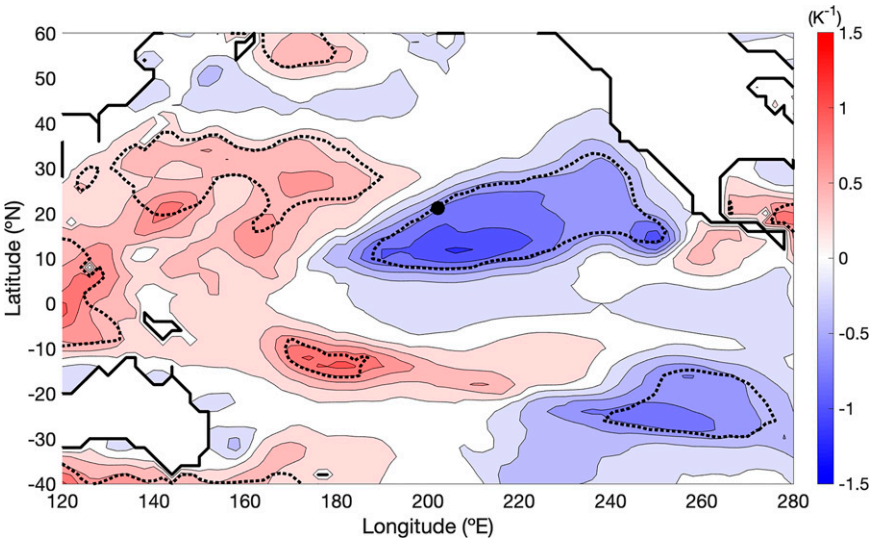

FIG. 11. Map of the coefficients of the linear regression between normalized δ^{18}O values from GNIP and SST anomalies. The dashed contours enclose areas where the correlation between the two variables is statistically significant at 95% confidence.

were interpreted as suggestive of an increased activity of Kona lows and cold fronts during certain time intervals. The observed lower δ^2H and δ^{18}O values in precipitation during disturbed periods are interpreted as due to the progressive rainout in the large-scale systems responsible for the precipitation and are consistent with other studies (Gedzelman and Lawrence 1990; Yoshimura et al. 2010; Risi et al. 2010; Pfahl et al. 2012; Kurita 2013; Aemisegger et al. 2015; Dütsch et al. 2016; Weng et al. 2021).

Considering that the climate in the Hawaiian Islands is dominated by trade winds, which blow with an easterly/northeasterly direction, a reasonable a priori expectation would be that rainfall collected on the windward side of the island is more enriched in ^{2}H and ^{18}O than that on the leeward side: as the airflow is lifted by the island orography, water vapor first condenses and then precipitation forms; as clouds continue their journey across the island, progressive rainout leads to lower δ^2H and δ^{18}O values in rainfall. The data presented in section 3, however, paint a more complex picture. Figure 4 suggests that precipitation at Lyon Arboretum—and, to some degree, also at Maunawili—appear to have much higher δ^2H and δ^{18}O values compared to the other sites.

The significantly higher δ^2H and δ^{18}O values recorded at Lyon Arboretum can be explained by three, possibly concurrent, factors. The first is the potential role of moisture that has evapotranspired from the soil or evaporated from canopy interception. Such a phenomenon, usually referred to as *moisture recycling*, has been observed in various locations around the world (e.g., Hildenbrand et al. 2005; Rhodes et al. 2006; Risi et al. 2013; Pfahl and Sodemann 2014; Otte et al. 2017; Sánchez-Murillo et al. 2017; Schmitt et al. 2018; Esquivel-Hernández et al. 2019), and it has been invoked to interpret some data collected in Hawai'i (Scholl et al. 2007; Booth et al. 2021). The moisture evaporating from the soil has relatively high δ^2H and δ^{18}O values, and its entrainment in a precipitating system will also lead to an increase of δ^2H and δ^{18}O values in precipitation. Lyon Arboretum is surrounded by vegetation and is immediately downwind from the steep ridges of the Ko'olau Mountain Range, which are also rich in vegetation. Taken together, these two factors suggest that Lyon Arboretum would be a favorable place to observe the effects of moisture recycling on the water isotopic composition of precipitation. In addition, Table 1 suggests that Lyon Arboretum is characterized by higher relative humidity than other sites, while Fig. 4 indicates that the precipitation at that site has relatively high deuterium excess values. Both of these factors have been used as indicators that moisture recycling plays an important role in explaining the isotopic composition of rainfall at a given site (Merlivat and Jouzel 1979; Scholl et al. 2007; Sánchez-Murillo et al. 2017; Schmitt et al. 2018). Moisture recycling might also be important in other sites, for example, at Maunawili, which is also situated in a highly vegetated area, and the high values of δ^2H, δ^{18}O, and deuterium excess during the dry season are consistent with this interpretation. The other three sites are in more urban locations, so the recycling of evapotranspired moisture is unlikely to be a significant factor there.

Another potential contributing factor to explain the higher δ^2H and δ^{18}O values at Lyon Arboretum is that different weather systems affect the five sites in different ways, due to their different windward and leeward locations across the Ko'olau Mountain Range, and they do not necessarily bring rainfall in proportional amounts to the five sites. For example, cold fronts and Kona lows, which are associated with low values of δ^2H and δ^{18}O, have a size and an intensity that likely affect the entire island of O'ahu, or at least substantial portions of it. On the other hand, trade-wind showers, which tend to have comparatively higher values of δ^2H and δ^{18}O than Kona low rainfall, are largely caused by the orographic lifting provided by the Ko'olau mountains. Because of the

easterly/northeasterly direction of the winds, trade-wind showers are likely to lead to large amounts of rain on the summits and immediately downwind of the mountains, where Lyon Arboretum is located. However, since the orographic lifting ceases after passing the mountain summits, and descent follows in the lee, many of these showers stop before reaching the HIG site. Thus, trade-wind showers affect Lyon Arboretum disproportionately compared to the rest of the network and cause the volume-weighted average to be higher than other places. Figure 5a shows that there is very little correlation between the rainfall collected at Lyon Arboretum and that collected at HIG, particularly during the dry season. Figure 5b suggests that a significant fraction of rain events that affected Lyon Arboretum did not affect HIG, especially during the dry season. Since the trade-wind shallow cumulus clouds that are formed by the orographic forcing typically lead to rainfall characterized by relatively high values of δ^2H and δ^{18}O, it is possible that the disproportionate number of events affecting Lyon Arboretum might contribute to explaining why the isotopic composition of precipitation there is significantly different than at other sites.

A third potential factor to interpret the data at Lyon Arboretum is the equilibration fractionation that takes place in the subcloud layer (Stewart 1975; Lee and Fung 2008; Aemisegger et al. 2015; Managave et al. 2016; Mercer et al. 2020; Graf et al. 2019; Vimeux and Risi 2021). Looking at the summary information in Table 1, it appears that Lyon Arboretum has a lower average annual temperature than all the other sites, in some cases by almost 2°C. The equilibrium fractionation ratio α^{eq} is a function of temperature and can be approximated by (Horita et al. 2008):

$$\alpha^{eq} = \exp\left(\frac{a}{T^2} + \frac{b}{T} + c\right), \tag{6}$$

where T is temperature, and $a = 24\,844$ (1137), $b = -76.248$ (-0.4156), and $c = 5.2612 \times 10^{-2}$ (-2.0667×10^{-3}) are semi-empirically determined constants for the ^{2}H (^{18}O) isotope (Horita et al. 2008). From this formula, there follows that

$$\frac{\partial \alpha^{eq}}{\partial T} = -\left(\frac{2a}{T^2} + \frac{b}{T}\right)\frac{\alpha^{eq}}{T}. \tag{7}$$

Assuming a temperature of 23.5°C (see Table 1), and assuming that the water vapor isotopic ratio, R_v, remains unchanged, Eq. (7) suggests that a decrease in temperature by 2°C would cause precipitation in equilibrium with the vapor to have higher δ^{18}O and δ^2H values by 0.17‰ and 2.24‰, respectively. Such a change likely affects the isotopic exchanges in the subcloud layer and contributes to explaining why δ^{18}O and δ^2H values are significantly higher than in other sites.

In addition, the expected pattern of decreasing δ^{18}O and δ^2H values across a mountain barrier assumes that airflow over the barrier is two-dimensional. However, the development of blocked flow may stall air upwind, and divert air around rather than over the barrier. Blocked flow can occur over the Koʻolau Range under low wind speeds, or high stability (high nondimensional mountain heights, e.g., Smith 1989; Galewsky 2009), and has been seen in observations and numerical models (Hsiao et al. 2021). During weak wind conditions, sea breezes are also likely (Zhang et al. 2005; Hsiao et al. 2020), drawing moisture sources from all directions, and resulting in uplift and precipitation that is not controlled by the orography and therefore could not have the expected windward to leeward isotopic pattern.

Another complicating factor is vertical mixing. In classic midlatitude orographic precipitation scenarios, the drying ratio (the fraction of the incoming water vapor flux that is rained out over the mountains) is as high as 40% or 50% (Smith and Evans 2007; Smith 2019). However, over tropical islands, it has been shown to be less than 0.5% (Smith et al. 2012). This drying ratio difference could have a significant impact on the evolution of δ^{18}O and δ^2H values. The differences between midlatitudes and the tropics come from the atmospheric stability and the vapor content. In the tropics, the conditionally unstable atmosphere drives vertical mixing once air is lifted above its lifting condensation level (LCL), resulting in a larger flux of moisture upward in the form of orographic convection rather than toward the surface in the form of rainfall. A leeside rain shadow can be caused by leeside descent, dry air entrainment, or increased static stability rather than airmass drying and progressive rainout (Smith et al. 2012). Similarly, the vertical convective motion mixes air from different airmasses such that precipitation is not produced only from air that originated in the boundary layer. These complicating factors are local in nature, and can also influence the isotopic pattern.

An important point that emerges from the systematic differences observed in the dataset, as well as with other extended network of sites in Hawai'i (Scholl et al. 2007; Dores et al. 2020), is that caution should be taken when using data from single sites in locations with complex topography. In the case of Hawai'i, for example, GNIP collected many years of data in a single location in Hilo, on the windward side of Hawai'i Island. If indeed, as suggested by Scholl et al. (2007) for Maui, windward locations experience stronger water vapor recycling in the presence of significant topography, isotope data in Hilo might have systematically different δ^2H and δ^{18}O values and higher deuterium excess than rainfall over the open ocean.

b. *The amount effect*

In the tropics, the amount effect is often used to interpret collected data. The results presented in this work suggest that the amount effect on Oʻahu is dependent on the location where precipitation is collected and on the sampling period. While Fig. 6f suggests a significant anticorrelation between δ^{18}O and rain rates at HIG and Kailua at all times, the anticorrelation appears insignificant for Maunawili and Lyon Arboretum during the dry season, and for Lyon Arboretum during nondisturbed periods. In addition, even when significantly different from 0, the correlation coefficients at Lyon Arboretum appear smaller than at other sites. The correlation also appears insignificant at Waikīkī for the wet season and for disturbed samples, but the scarcity of observations there is likely responsible for that.

As discussed in section 1, the amount effect is not a feature that has been universally observed, and a number of high-frequency collections in tropical sites have been conducted through the years where no significant correlation was observed between the rainfall isotopic composition and rain rates (Rhodes et al. 2006; Uemura et al. 2012; Moerman et al. 2013; Windhorst et al. 2013; Scholl and Murphy 2014; Conroy et al. 2016b; Permana et al. 2016; Schmitt et al. 2018). Compared to some of the studies where the amount effect was not observed, the results presented in this work are characterized by great spatial variability, even when comparing results sampled with the same frequency.

One potential explanation for why Lyon Arboretum shows smaller, sometimes insignificant correlations between rainfall isotopic composition and rain rates is that orographically generated rain might not experience the same degree of rainout as rain from large-scale systems (Liu et al. 2005; Rhodes et al. 2006; Scholl et al. 2009). After all, Lyon Arboretum is particularly close to the Koʻolau Mountain Range, and the site is more affected by orographic rain than other sites (Fig. 5b). One factor that might increase the anticorrelation at other sites, as particularly visible for HIG in Figs. 6c and 6e, is that rain might experience significant subcloud rain evaporation before being collected. This could cause higher $\delta^{18}O$ values (and lower deuterium excess values) at lower rain rate percentiles at some sites.

c. *Seasonal variability*

While Fig. 4c suggests that differences in the volume-weighted averages of deuterium excess values between wet and dry season are not significant at most sites, the time series shown in Fig. 2d suggests that there are seasonal variations at all the sites. Consistent with other observations across the planet (Araguás-Araguás et al. 2000; Delmotte et al. 2000; Rhodes et al. 2006; Yoshimura and Ichiyanagi 2009; Guan et al. 2013; Pfahl and Sodemann 2014; Scholl and Murphy 2014; Kopec et al. 2019), this behavior for data in Hawaiʻi is interpreted as being caused by changes in the air masses that contribute to precipitation at different times of the year: while synoptic systems that are responsible for much of the rainfall during the wet season originate in the northwestern Pacific (Kodama and Barnes 1997; Kodama and Businger 1998), rainfall during the dry season is mostly due to the trade-wind flow, which originates in the northeastern part of the Pacific basin (see Fig. 8).

Figure 9 suggests that the different geographical origin and the seasonal cycle make air parcels that contribute to rainfall on Oʻahu experience different thermodynamic environments. In particular, Fig. 8c shows that the median time of last entry—the time prior to a trajectory's arrival on Oʻahu when it descends below the boundary layer—is 3.25 days, with little seasonal difference. If trajectories spend a considerable amount of time in the boundary layer, it is likely that they experience significant mixing with boundary layer vapor, and thus are very sensitive to the environmental conditions near the Hawaiian Islands. A series of studies have tried to link the deuterium excess values to the thermodynamic environment where evaporation takes place and, while there still is some debate on the subject (Pfahl and Sodemann 2014), an anticorrelation has been shown between near-surface relative humidity and deuterium excess values of water vapor evaporated from the ocean (Merlivat and Jouzel 1979; Johnsen et al. 1989; Uemura et al. 2008; Pfahl and Sodemann 2014). Figure 9a shows that trajectories in the boundary layer experience higher relative humidity during the dry season compared to the wet season, which would lead to lower deuterium excess values in the vapor sourced from the ocean. On the other hand, trajectories also experience a higher SST during the dry season, and a positive correlation has been shown between deuterium excess values in water vapor and SST, although this seems to be weak on synoptic time scales (Pfahl and Sodemann 2014).

Using the correlation coefficients determined by Johnsen et al. (1989), the differences in relative humidity and SST would lead to an average difference of $-0.82‰$ between the dry and the wet season values of deuterium excess of the water vapor evaporated from the ocean. The difference would become $-1.62‰$ if only relative humidity was taken into account. The average is taken considering near surface values of relative humidity and SST between 1 and 3 days prior to a trajectory's arrival on Oʻahu. The relation proposed by Uemura et al. (2008) would lead to similar, albeit smaller, values ($-0.56‰$).

In addition to the different properties of the water vapor that an incoming trajectory might mix with, the original values of deuterium excess might also be different across seasons. For example, the values of water vapor deuterium excess predicted by Pfahl and Sodemann (2014, see their Fig. 2) in the western Pacific region during the winter months (DJF) are much higher than those in the central and eastern Pacific during the summer months (JJA). Considering the different origins of the trajectories affecting Oʻahu at different times of year (Fig. 8), this could be another factor to explain the observed seasonal differences.

This discussion suggests a connection between the deuterium excess found in rainfall in Hawaiʻi and the large-scale dynamics that influence the climate in the North Pacific region. In principle, this connection could be used to diagnose, or at least provide further constraints on those dynamics at times for which there was insufficient coverage of meteorological data, for example when the GNIP site in Hilo was active, or in the interpretation of paleoclimate data, assuming that both $\delta^{18}O$ and $\delta^{2}H$ values are available.

On a more local scale, another potential contributing factor that would lead to seasonal changes of deuterium excess are differences in rain evaporation that precipitating columns experience in different seasons. The blue and red curves in Fig. S5 show the diurnal cycle of the average relative humidity at Lyon Arboretum during the wet and the dry season, respectively. In spite of the similarities between the two curves, relative humidity values during the dry season are lower than the wet-season curve by 4%–5%. This is particularly evident in the afternoon/evening, when a peak in rainfall from trade-wind showers is often observed in many locations across the island (Hartley and Chen 2010). Assuming that the size spectrum of raindrops does not vary too much throughout the year, rain that falls during the dry season should experience more rain evaporation, resulting

in lower deuterium excess in precipitation. This could help explain differences observed between deuterium excess values across the sites.

d. Interannual variability

To place the LMWL computed in section 3 in context, the values of the slope and the intercept are compared in Fig. 7 with other LMWLs computed in Hawai'i (McMurtry et al. 1977; Scholl et al. 1996, 2002; Fackrell and Glenn 2014; Dores et al. 2020; Booth et al. 2021; Fackrell et al. 2020; Tachera et al. 2021). The slopes and the intercepts of all these measurements appear distributed on a relatively wide range, even for collections that were close in time and conducted on the same island: for example, the slope determined by Dores et al. (2020) on O'ahu is 3σ away from the slope determined in section 3. Based on some of the results presented here, and judging by the differences between the LMWL computed from windward data and leeward data only (Fig. 7), one might argue that geographical differences in the location of the sites might be responsible for the observed discrepancies. However, the LMWLs determined by Fackrell et al. (2020) and Tachera et al. (2021) on the same portion of Hawai'i Island appear quite different. It is thus natural to wonder whether interannual variability might also play a role.

While most of the collections conducted in Hawai'i span at most 2 years and are therefore insufficient to draw any robust conclusions, the data from GNIP at Hilo might provide some insight. Figures 10a and 10b show that monthly means of δ^{18}O and δ^{2}H values exhibit great interannual variability, particularly during the wet season, with some years characterized by very negative values and others by positive ones. Figure 10c further suggests that the LMWL using data collected over one year might be susceptible to appreciable, though not statistically significant, differences.

Some insights on what might be driving the interannual variability could be gained from Fig. 11, which links the δ^{18}O values in precipitation at Hilo with global SSTs. The figure suggests an overall positive correlation with the western Pacific warm pool and a negative correlation with SSTs in the eastern Pacific. To some degree, the correlation resembles the ENSO pattern (Rasmusson and Carpenter 1982). This is perhaps not surprising considering the influence that ENSO has on climate in Hawai'i (Chu and Chen 2005; Frazier et al. 2018). In their recent analysis, Longman et al. (2021) have shown that positive phases of ENSO are associated with significantly more cold fronts, although these do not necessarily lead to an increase in rainfall. Precipitation from cold fronts could experience considerably more rainout compared to trade-wind showers, and this could lead to lower δ^{18}O values in the accumulated precipitation. The correlation between δ^{18}O values and SST appears much weaker during the dry season than the wet season (Figs. S3 and S4), which might explain why dry-season values of δ^{18}O and δ^{2}H exhibit a smaller interannual variability than wet-season values.

The above analysis is not meant to show rigorous evidence of a clear relationship between rainfall isotopic composition and the large-scale climate forcing, but, merely to provide a suggestion that such a relationship might exist, and that more work is needed. This would be a particularly significant finding, for example, since most of the data collection in Hawai'i that has been used to compute LMWLs and estimate aquifer recharge times is typically limited to 1 or 2 years. As Putman et al. (2019) recently pointed out, however, the correct determination of a LMWL in any particular region requires a collection on time scales at least as long as those of the processes controlling the variability. In the case of Hawai'i, this could imply the necessity of time series that span multiple years, possibly decades.

The increased collection frequency of the data presented here allows a clearer understanding of the isotopic composition and the origin of the systems responsible for precipitation on the islands. Furthermore, even though the dataset is limited to the island of O'ahu, the main results are likely applicable to other mountainous islands in the Pacific region. Some of these islands, such as Tahiti, are located at similar latitudes and are also characterized by orographic profiles that are not dissimilar to the ones found in Hawai'i.

At the same time, however, there are three main limitations to this study. First, weekly collections might not be sufficient for some process-based studies or, for example, to assess what causes day-to-day differences in the isotopic composition of trade-wind rainfall. Furthermore, the network of sites is quite spatially limited and, given how much δ^{18}O and δ^{2}H values as well as deuterium excess can vary within the network, it leaves the open question of the spatial variability across O'ahu and, more generally, the Hawaiian Archipelago. Finally, the interannual variability suggests that even a 2-yr collection might be insufficient to obtain a clear picture of rainfall water isotopic composition in Hawai'i. Maintaining a long-time data collection over an extended region is very challenging, particularly at this historic time, but efforts are underway to overcome the limitations and increase the potential of the isotope network in Hawai'i that has been established.

5. Conclusions

The results presented in this work highlight the variability of rainfall isotopic composition in a region characterized by complex topography, such as a mountainous tropical island. The significant differences in the volume-weighted averages suggest a large degree of spatial heterogeneity in the results. In addition, the lack of a statistically significant anticorrelation between δ^{18}O values and rain rates at Lyon Arboretum and Maunawili for certain sampling periods (dry season and nondisturbed weeks) also illustrates the limitations of the amount effect as an interpretative lens of tropical rainfall isotopic composition. Variability was also observed in the temporal domain, with appreciable seasonal differences in deuterium excess at all sites, and also with differences in monthly δ^{18}O and δ^{2}H values from year to year. The analyses presented here revealed that these changes could be related to the larger scale: seasonal differences in atmospheric circulation and thermodynamic conditions in the former case, and broader climatic changes in the latter.

Although a number of potential factors have been invoked to explain the data collected, more data will be needed to draw definitive conclusions. Efforts are ongoing to improve on the existing network by including measurements of water vapor isotopes and to conduct high-resolution numerical simulations using isotope-enabled regional models. In a broader context, because the isotopic composition of rainfall has often been used to study islands' groundwater resources or the climate in important regions such as the Pacific, the data in this work and their spatial and temporal variability highlight the need for increased long-term efforts to monitor the isotopic composition of rainfall across the world.

Acknowledgments. We would like to express our gratitude to the staff of the Lyon Arboretum for granting us the permission to collect water on their grounds, and for working with us during the COVID-19 pandemic, even at times when the arboretum was closed to the public. We would also like to thank Creighton Litton, John Bravender, Nicole C. Popp, and Jan Reichelderfer for generously agreeing to help in collecting weekly rainfall samples. The data collection would have been impossible without all the passion and hard work that undergraduate students in the Department of Atmospheric Sciences Britt Seifert, Eleanore Law, and John (Jack) Fast put into this project, and to them goes our most heartfelt gratitude. The technical support and advanced computing resources from University of Hawai'i Information Technology Services – Cyberinfrastructure, funded in part by the National Science Foundation MRI Award 1920304, are also gratefully acknowledged. Finally, we want to thank Ryan Longman, Thomas Giambelluca, Yin-Phan Tsang, Malte Stuecker, and Peter Huybers for enlightening discussions. G.T. was partially supported by the National Science Foundation Grant AGS-1945972. The undergraduate students and the equipment purchased for this project were supported by the Undergraduate Research Opportunities Program at the University of Hawai'i at Mānoa. This is SOEST Contribution Number 11653.

Data availability statement. The data used in this paper are available at https://doi.org/10.5281/zenodo.7809301.

REFERENCES

Aemisegger, F., 2018: On the link between the North Atlantic storm track and precipitation deuterium excess in Reykjavik. *Atmos. Sci. Lett.*, **19**, e865, https://doi.org/10.1002/asl.865.

——, S. Pfahl, H. Sodemann, I. Lehner, S. I. Seneviratne, and H. Wernli, 2014: Deuterium excess as a proxy for continental moisture recycling and plant transpiration. *Atmos. Chem. Phys.*, **14**, 4029–4054, https://doi.org/10.5194/acp-14-4029-2014.

——, J. K. Spiegel, S. Pfahl, H. Sodemann, W. Eugster, and H. Wernli, 2015: Isotope meteorology of cold front passages: A case study combining observations and modeling. *Geophys. Res. Lett.*, **42**, 5652–5660, https://doi.org/10.1002/2015GL063988.

Araguás-Araguás, L., K. Froehlich, and K. Rozanski, 2000: Deuterium and oxygen-18 isotope composition of precipitation and atmospheric moisture. *Hydrol. Processes*, https://doi.org/10.1002/1099-1085(20000615)14:8<1341::AID-HYP983>3.0.CO;2-Z.

Bailey, A., J. Nusbaumer, and D. Noone, 2015: Precipitation efficiency derived from isotope ratios in water vapor distinguishes dynamical and microphysical influences on subtropical atmospheric constituents. *J. Geophys. Res. Atmos.*, **120**, 9119–9137, https://doi.org/10.1002/2015JD023403.

Barras, V., and I. Simmonds, 2009: Observation and modeling of stable water isotopes as diagnostics of rainfall dynamics over southeastern Australia. *J. Geophys. Res.*, **114**, D23308, https://doi.org/10.1029/2009JD012132.

Beilman, D. W., C. Massa, J. E. Nichols, O. Elison Timm, R. Kallstrom, and S. Dunbar-Co, 2019: Dynamic Holocene vegetation and North Pacific hydroclimate recorded in a mountain peatland, Moloka'i, Hawai'i. *Front. Earth Sci.*, **7**, 188, https://doi.org/10.3389/feart.2019.00188.

Booth, H., N. Lautze, D. Tachera, and D. Dores, 2021: Event-based stable isotope analysis of precipitation along a high resolution transect on the south face of O'ahu, Hawai'i. *Pac. Sci.*, **75**, 421–441, https://doi.org/10.2984/75.3.9.

Bowen, G. J., Z. Cai, R. P. Fiorella, and A. L. Putman, 2019: Isotopes in the water cycle: Regional- to global-scale patterns and applications. *Annu. Rev. Earth Planet. Sci.*, **47**, 453–479, https://doi.org/10.1146/annurev-earth-053018-060220.

Burns, S. J., A. Matter, N. Frank, and A. Mangini, 1998: Speleothem-based paleoclimate record from northern Oman. *Geology*, **26**, 499–502, https://doi.org/10.1130/0091-7613(1998)026<0499:SBPRFN>2.3.CO;2.

Cao, G., T. W. Giambelluca, D. E. Stevens, and T. A. Schroeder, 2007: Inversion variability in the Hawaiian trade wind regime. *J. Climate*, **20**, 1145–1160, https://doi.org/10.1175/JCLI4033.1.

Carreira, P. M., J. M. Marques, A. Pina, A. Mota Gomes, P. A. Galego Fernandes, and F. Monteiro Santos, 2010: Groundwater assessment at Santiago Island (Cabo Verde): A multidisciplinary approach to a recurring source of water supply. *Water Resour. Manage.*, **24**, 1139–1159, https://doi.org/10.1007/s11269-009-9489-z.

Chu, P.-S., and H. Chen, 2005: Interannual and interdecadal rainfall variations in the Hawaiian Islands. *J. Climate*, **18**, 4796–4813, https://doi.org/10.1175/JCLI3578.1.

Conroy, J. L., K. M. Cobb, and D. Noone, 2016a: Manus water isotope investigation field campaign report. Tech. Rep. DOE/SC-ARM-15-079, 14 pp., https://www.osti.gov/biblio/1251149.

——, D. Noone, K. M. Cobb, J. W. Moerman, and B. L. Konecky, 2016b: Paired stable isotopologues in precipitation and vapor: A case study of the amount effect within western tropical pacific storms. *J. Geophys. Res. Atmos.*, **121**, 3290–3303, https://doi.org/10.1002/2015JD023844.

Craig, H., 1961: Isotopic variations in meteoric waters. *Science*, **133**, 1702–1703, https://doi.org/10.1126/science.133.3465.1702.

Dahinden, F., and Coauthors, 2021: Disentangling different moisture transport pathways over the eastern subtropical North Atlantic using multi-platform isotope observations and high-resolution numerical modelling. *Atmos. Chem. Phys.*, **21**, 16 319–16 347, https://doi.org/10.5194/acp-21-16319-2021.

Dansgaard, W., 1964: Stable isotopes in precipitation. *Tellus*, **16**, 436–468, https://doi.org/10.1111/j.2153-3490.1964.tb00181.x.

Delmotte, M., V. Masson, J. Jouzel, and V. I. Morgan, 2000: A seasonal deuterium excess signal at law dome, coastal eastern Antarctica: A Southern Ocean signature. *J. Geophys. Res.*, **105**, 7187–7197, https://doi.org/10.1029/1999JD901085.

Dores, D., C. R. Glenn, G. Torri, R. B. Whittier, and B. N. Popp, 2020: Implications for groundwater recharge from stable isotopic composition of precipitation in Hawai'i during the 2017–2018 La Niña. *Hydrol. Processes*, **34**, 4675–4696, https://doi.org/10.1002/hyp.13907.

Draxler, R., and G. Hess, 1998: An overview of the hysplit$_4$ modeling system for trajectories, dispersion, and deposition. *Aust. Meteor. Mag.*, **47**, 295–308.

Dütsch, M., S. Pfahl, and H. Wernli, 2016: Drivers of δ^2H variations in an idealized extratropical cyclone. *Geophys. Res. Lett.*, **43**, 5401–5408, https://doi.org/10.1002/2016GL068600.

Esquivel-Hernández, G., and Coauthors, 2019: Moisture transport and seasonal variations in the stable isotopic composition of rainfall in Central American and Andean Páramo during El Niño conditions (2015–2016). *Hydrol. Processes*, **33**, 1802–1817, https://doi.org/10.1002/hyp.13438.

Fackrell, J., and C. Glenn, 2014: How much do high-level aquifers impact SGD and the coastal zone in Hawai'i? Unscrambling the mix with water isotopes. *2014 Ocean Sciences Meeting*, Honolulu, HI, Amer. Geophys. Union, 1068.

Fackrell, J. K., C. R. Glenn, D. Thomas, R. Whittier, and B. N. Popp, 2020: Stable isotopes of precipitation and groundwater provide new insight into groundwater recharge and flow in a structurally complex hydrogeologic system: West Hawai'i, USA. *Hydrogeol. J.*, **28**, 1191–1207, https://doi.org/10.1007/s10040-020-02143-9.

Frappier, A., D. Sahagian, L. A. González, and S. J. Carpenter, 2002: El Niño events recorded by stalagmite carbon isotopes. *Science*, **298**, 565, https://doi.org/10.1126/science.1076446.

Frappier, A. B., D. Sahagian, S. J. Carpenter, L. A. González, and B. R. Frappier, 2007: Stalagmite stable isotope record of recent tropical cyclone events. *Geology*, **35**, 111–114, https://doi.org/10.1130/G23145A.1.

Frazier, A. G., O. Elison Timm, T. W. Giambelluca, and H. F. Diaz, 2018: The influence of ENSO, PDO and PNA on secular rainfall variations in Hawai'i. *Climate Dyn.*, **51**, 2127–2140, https://doi.org/10.1007/s00382-017-4003-4.

Friedman, I., and A. H. Woodcock, 1957: Determination of deuterium-hydrogen ratios in Hawaiian waters. *Tellus*, **9**, 553–556, https://doi.org/10.3402/tellusa.v9i4.9119.

Froehlich, K., J. J. Gibson, and P. K. Aggarwal, 2002: Deuterium excess in precipitation and its climatological significance. Tech. Rep. IAEA-CSP–13/P, International Atomic Energy Agency, 13 pp., https://inis.iaea.org/search/search.aspx?orig_q=RN:34017972.

Galewsky, J., 2009: Rain shadow development during the growth of mountain ranges: An atmospheric dynamics perspective. *J. Geophys. Res.*, **114**, F01018, https://doi.org/10.1029/2008JF001085.

——, H. C. Steen-Larsen, R. D. Field, J. Worden, C. Risi, and M. Schneider, 2016: Stable isotopes in atmospheric water vapor and applications to the hydrologic cycle. *Rev. Geophys.*, **54**, 809–865, https://doi.org/10.1002/2015RG000512.

Gedzelman, S. D., and J. R. Lawrence, 1990: The isotopic composition of precipitation from two extratropical cyclones. *Mon. Wea. Rev.*, **118**, 495–509, https://doi.org/10.1175/1520-0493(1990)118<0495:TICOPF>2.0.CO;2.

Giambelluca, T. W., Q. Chen, A. G. Frazier, J. P. Price, Y.-L. Chen, P.-S. Chu, J. K. Eischeid, and D. M. Delparte, 2013: Online rainfall atlas of Hawai'i. *Bull. Amer. Meteor. Soc.*, **94**, 313–316, https://doi.org/10.1175/BAMS-D-11-00228.1.

Giambelluca, T., and Coauthors, 2014: Evapotranspiration of Hawai'i. Final Rep., 178 pp., http://evapotranspiration.geography.hawaii.edu/assets/files/PDF/ET%20Project%20Final%20Report.pdf.

Gingerich, S., and D. S. Oki, 2000: Ground water in Hawai'i. U.S. Geological Survey, 6 pp., https://pubs.usgs.gov/fs/2000/126/pdf/fs126-00.pdf.

Goldberg, L. R., A. N. Kercheval, and K. Lee, 2005: *t*-statistics for weighted means in credit risk modeling. *J. Risk Finance*, **6**, 349–365, https://doi.org/10.1108/15265940510613688.

González, Y., and Coauthors, 2016: Detecting moisture transport pathways to the subtropical North Atlantic free troposphere using paired H_2O-δD in situ measurements. *Atmos. Chem. Phys.*, **16**, 4251–4269, https://doi.org/10.5194/acp-16-4251-2016.

Graf, P., H. Wernli, S. Pfahl, and H. Sodemann, 2019: A new interpretative framework for below-cloud effects on stable water isotopes in vapour and rain. *Atmos. Chem. Phys.*, **19**, 747–765, https://doi.org/10.5194/acp-19-747-2019.

Gröning, M., H. O. Lutz, Z. Roller-Lutz, M. Kralik, L. Gourcy, and L. Pöltenstein, 2012: A simple rain collector preventing water re-evaporation dedicated for δ^{18}O and δ^2H analysis of cumulative precipitation samples. *J. Hydrol.*, **448–449**, 195–200, https://doi.org/10.1016/j.jhydrol.2012.04.041.

Guan, H., X. Zhang, G. Skrzypek, Z. Sun, and X. Xu, 2013: Deuterium excess variations of rainfall events in a coastal area of South Australia and its relationship with synoptic weather systems and atmospheric moisture sources. *J. Geophys. Res. Atmos.*, **118**, 1123–1138, https://doi.org/10.1002/jgrd.50137.

Guilpart, E., F. Vimeux, S. Evan, J. Brioude, J.-M. Metzger, C. Barthe, C. Risi, and O. Cattani, 2017: The isotopic composition of near-surface water vapor at the Maïdo observatory (reunion island, southwestern Indian Ocean) documents the controls of the humidity of the subtropical troposphere. *J. Geophys. Res. Atmos.*, **122**, 9628–9650, https://doi.org/10.1002/2017JD026791.

Gupta, P., D. Noone, J. Galewsky, C. Sweeney, and B. H. Vaughn, 2009: Demonstration of high-precision continuous measurements of water vapor isotopologues in laboratory and remote field deployments using wavelength-scanned cavity ring-down spectroscopy (WS-CRDS) technology. *Rapid Commun. Mass Spectrom.*, **23**, 2534–2542, https://doi.org/10.1002/rcm.4100.

Hartley, T. M., and Y.-L. Chen, 2010: Characteristics of summer trade wind rainfall over Oahu. *Wea. Forecasting*, **25**, 1797–1815, https://doi.org/10.1175/2010WAF2222328.1.

He, S., N. F. Goodkin, N. Kurita, X. Wang, and C. M. Rubin, 2018: Stable isotopes of precipitation during tropical sumatra squalls in Singapore. *J. Geophys. Res. Atmos.*, **123**, 3812–3829, https://doi.org/10.1002/2017JD027829.

Heilweil, V. M., D. K. Solomon, S. B. Gingerich, and I. M. Verstraeten, 2009: Oxygen, hydrogen, and helium isotopes for investigating groundwater systems of the Cape Verde Islands, West Africa. *Hydrogeol. J.*, **17**, 1157–1174, https://doi.org/10.1007/s10040-009-0434-2.

Herrera, C., and E. Custodio, 2008: Conceptual hydrogeological model of volcanic Easter Island (Chile) after chemical and isotopic surveys. *Hydrogeol. J.*, **16**, 1329–1348, https://doi.org/10.1007/s10040-008-0316-z.

Hersbach, H., and Coauthors, 2019: Global reanalysis: Goodbye era-interim, hello ERA5. *ECMWF Newsletter*, No. 159, ECMWF, Reading, United Kingdom, 17–24, https://doi.org/10.21957/vf291hehd7.

Hildenbrand, A., C. Marlin, A. Conroy, P.-Y. Gillot, A. Filly, and M. Massault, 2005: Isotopic approach of rainfall and groundwater circulation in the volcanic structure of Tahiti-Nui

(French Polynesia). *J. Hydrol.*, **302**, 187–208, https://doi.org/10.1016/j.jhydrol.2004.07.006.

Horita, J., K. Rozanski, and S. Cohen, 2008: Isotope effects in the evaporation of water: A status report of the Craig–Gordon model. *Isot. Environ. Health Stud.*, **44**, 23–49, https://doi.org/10.1080/10256010801887174.

Hsiao, F., Y.-L. Chen, and D. E. Hitzl, 2020: Heavy rainfall events over central Oahu under weak wind conditions during seasonal transitions. *Mon. Wea. Rev.*, **148**, 4117–4141, https://doi.org/10.1175/MWR-D-19-0358.1.

——, ——, H. V. Nguyen, D. E. Hitzl, and R. Ballard, 2021: Effects of trade wind strength on airflow and cloudiness over Oahu. *Mon. Wea. Rev.*, **149**, 3037–3062, https://doi.org/10.1175/MWR-D-20-0399.1.

Huang, B., and Coauthors, 2017: NOAA extended reconstructed sea surface temperature (ERSST), version 5/. NOAA National Centers for Environmental Information, accessed 12 September 2021, https://doi.org/10.7289/V5T72FNM.

IAEA/WMO, 2021: Global network of isotopes in precipitation. The GNIP database. https://www.iaea.org/services/networks/gnip.

Johnsen, S. J., W. Dansgaard, and J. W. C. White, 1989: The origin of Arctic precipitation under present and glacial conditions. *Tellus*, **41B**, 452–468, https://doi.org/10.3402/tellusb.v41i4.15100.

Kelly, J. L., and C. R. Glenn, 2015: Chlorofluorocarbon apparent ages of groundwaters from west Hawaii, USA. *J. Hydrol.*, **527**, 355–366, https://doi.org/10.1016/j.jhydrol.2015.04.069.

Kodama, K. R., and G. M. Barnes, 1997: Heavy rain events over the south-facing slopes of Hawaii: Attendant conditions. *Wea. Forecasting*, **12**, 347–367, https://doi.org/10.1175/1520-0434(1997)012<0347:HREOTS>2.0.CO;2.

——, and S. Businger, 1998: Weather and forecasting challenges in the Pacific region of the national weather service. *Wea. Forecasting*, **13**, 523–546, https://doi.org/10.1175/1520-0434(1998)013<0523:WAFCIT>2.0.CO;2.

Kopec, B. G., X. Feng, E. S. Posmentier, and L. J. Sonder, 2019: Seasonal deuterium excess variations of precipitation at Summit, Greenland, and their climatological significance. *J. Geophys. Res. Atmos.*, **124**, 72–91, https://doi.org/10.1029/2018JD028750.

Kurita, N., 2013: Water isotopic variability in response to mesoscale convective system over the tropical ocean. *J. Geophys. Res. Atmos.*, **118**, 10 376–10 390, https://doi.org/10.1002/jgrd.50754.

——, K. Ichiyanagi, J. Matsumoto, M. D. Yamanaka, and T. Ohata, 2009: The relationship between the isotopic content of precipitation and the precipitation amount in tropical regions. *J. Geochem. Explor.*, **102**, 113–122, https://doi.org/10.1016/j.gexplo.2009.03.002.

Lee, J.-E., and I. Fung, 2008: "Amount effect" of water isotopes and quantitative analysis of post-condensation processes. *Hydrol. Processes*, **22**, 1–8, https://doi.org/10.1002/hyp.6637.

——, ——, D. J. DePaolo, and C. C. Henning, 2007: Analysis of the global distribution of water isotopes using the NCAR atmospheric general circulation model. *J. Geophys. Res.*, **112**, D16306, https://doi.org/10.1029/2006JD007657.

Leroy-Dos Santos, C., and Coauthors, 2020: A 4.5 year-long record of Svalbard water vapor isotopic composition documents winter air mass origin. *J. Geophys. Res. Atmos.*, **125**, e2020JD032681, https://doi.org/10.1029/2020JD032681.

Liu, W. J., Y. Ping Zhang, H. Mei Li, and Y. Hong Liu, 2005: Fog drip and its relation to groundwater in the tropical seasonal rain forest of Xishuangbanna, Southwest China: A preliminary study. *Water Res.*, **39**, 787–794, https://doi.org/10.1016/j.watres.2004.12.002.

Longman, R. J., H. F. Diaz, and T. W. Giambelluca, 2015: Sustained increases in lower-tropospheric subsidence over the central tropical North Pacific drive a decline in high-elevation rainfall in Hawaii. *J. Climate*, **28**, 8743–8759, https://doi.org/10.1175/JCLI-D-15-0006.1.

——, O. E. Timm, T. W. Giambelluca, and L. Kaiser, 2021: A 20-year analysis of disturbance-driven rainfall on O'ahu, Hawai'i. *Mon. Wea. Rev.*, **149**, 1767–1783, https://doi.org/10.1175/MWR-D-20-0287.1.

Managave, S. R., R. A. Jani, T. Narayana Rao, K. Sunilkumar, S. Satheeshkumar, and R. Ramesh, 2016: Intra-event isotope and raindrop size data of tropical rain reveal effects concealed by event averaged data. *Climate Dyn.*, **47**, 981–987, https://doi.org/10.1007/s00382-015-2884-7.

Mandal, A. K., J. Zhang, and K. Asai, 2011: Stable isotopic and geochemical data for inferring sources of recharge and groundwater flow on the volcanic island of Rishiri, Japan. *Appl. Geochem.*, **26**, 1741–1751, https://doi.org/10.1016/j.apgeochem.2011.05.001.

Mantua, N. J., S. R. Hare, Y. Zhang, J. M. Wallace, and R. C. Francis, 1997: A Pacific interdecadal climate oscillation with impacts on salmon production. *Bull. Amer. Meteor. Soc.*, **78**, 1069–1080, https://doi.org/10.1175/1520-0477(1997)078<1069:APICOW>2.0.CO;2.

Martin, N. J., J. L. Conroy, D. Noone, K. M. Cobb, B. L. Konecky, and S. Rea, 2018: Seasonal and ENSO influences on the stable isotopic composition of Galápagos precipitation. *J. Geophys. Res. Atmos.*, **123**, 261–275, https://doi.org/10.1002/2017JD027380.

Massa, C., D. W. Beilman, J. E. Nichols, and O. E. Timm, 2021: Central Pacific hydroclimate over the last 45,000 years: Molecular-isotopic evidence from leaf wax in a Hawai'i peatland. *Quat. Sci. Rev.*, **253**, 106744, https://doi.org/10.1016/j.quascirev.2020.106744.

McMurtry, G. M., P.-F. Fan, and T. B. Coplen, 1977: Chemical and isotopic investigations of groundwater in potential geothermal areas in Hawaii. *Amer. J. Sci.*, **277**, 438–458, https://doi.org/10.2475/ajs.277.4.438.

Mercer, J. J., D. T. Liefert, and D. G. Williams, 2020: Atmospheric vapour and precipitation are not in isotopic equilibrium in a continental mountain environment. *Hydrol. Processes*, **34**, 3078–3101, https://doi.org/10.1002/hyp.13775.

Merlivat, L., and J. Jouzel, 1979: Global climatic interpretation of the deuterium-oxygen 18 relationship for precipitation. *J. Geophys. Res.*, **84**, 5029–5033, https://doi.org/10.1029/JC084iC08p05029.

Moerman, J. W., K. M. Cobb, J. F. Adkins, H. Sodemann, B. Clark, and A. A. Tuen, 2013: Diurnal to interannual rainfall $\delta^{18}O$ variations in Northern Borneo driven by regional hydrology. *Earth Planet. Sci. Lett.*, **369–370**, 108–119, https://doi.org/10.1016/j.epsl.2013.03.014.

Moore, M., Z. Kuang, and P. N. Blossey, 2014: A moisture budget perspective of the amount effect. *Geophys. Res. Lett.*, **41**, 1329–1335, https://doi.org/10.1002/2013GL058302.

Murakami, H., B. Wang, T. Li, and A. Kitoh, 2013: Projected increase in tropical cyclones near Hawaii. *Nat. Climate Change*, **3**, 749–754, https://doi.org/10.1038/nclimate1890.

Otte, I., F. Detsch, A. Gütlein, M. Scholl, R. Kiese, T. Appelhans, and T. Nauss, 2017: Seasonality of stable isotope composition of atmospheric water input at the southern slopes of Mt. Kilimanjaro, Tanzania. *Hydrol. Processes*, **31**, 3932–3947, https://doi.org/10.1002/hyp.11311.

Papritz, L., F. Aemisegger, and H. Wernli, 2021: Sources and transport pathways of precipitating waters in cold-season

deep North Atlantic cyclones. *J. Atmos. Sci.*, **78**, 3349–3368, https://doi.org/10.1175/JAS-D-21-0105.1.

Permana, D. S., L. G. Thompson, and G. Setyadi, 2016: Tropical west pacific moisture dynamics and climate controls on rainfall isotopic ratios in southern Papua, Indonesia. *J. Geophys. Res. Atmos.*, **121**, 2222–2245, https://doi.org/10.1002/2015JD023893.

Pfahl, S., and H. Sodemann, 2014: What controls deuterium excess in global precipitation? *Climate Past*, **10**, 771–781, https://doi.org/10.5194/cp-10-771-2014.

——, H. Wernli, and K. Yoshimura, 2012: The isotopic composition of precipitation from a winter storm–A case study with the limited-area model $\text{cosmo}_{\text{iso}}$. *Atmos. Chem. Phys.*, **12**, 1629–1648, https://doi.org/10.5194/acp-12-1629-2012.

Prada, S., J. V. Cruz, and C. Figueira, 2016: Using stable isotopes to characterize groundwater recharge sources in the volcanic island of Madeira, Portugal. *J. Hydrol.*, **536**, 409–425, https://doi.org/10.1016/j.jhydrol.2016.03.009.

Putman, A. L., R. P. Fiorella, G. J. Bowen, and Z. Cai, 2019: A global perspective on local meteoric water lines: Meta-analytic insight into fundamental controls and practical constraints. *Water Resour. Res.*, **55**, 6896–6910, https://doi.org/10.1029/2019WR025181.

Rasmusson, E. M., and T. H. Carpenter, 1982: Variations in tropical sea surface temperature and surface wind fields associated with the Southern Oscillation/El Niño. *Mon. Wea. Rev.*, **110**, 354–384, https://doi.org/10.1175/1520-0493(1982)110<0354:VITSST>2.0.CO;2.

Rhodes, A. L., A. J. Guswa, and S. E. Newell, 2006: Seasonal variation in the stable isotopic composition of precipitation in the tropical montane forests of Monteverde, Costa Rica. *Water Resour. Res.*, **42**, W11402, https://doi.org/10.1029/2005WR004535.

Ricker, W. E., 1973: Linear regressions in fishery research. *J. Fish. Res. Board Canada*, **30**, 409–434, https://doi.org/10.1139/f73-072.

Risi, C., S. Bony, and F. Vimeux, 2008: Influence of convective processes on the isotopic composition (δ^{18}O and δD) of precipitation and water vapor in the tropics: 2. Physical interpretation of the amount effect. *J. Geophys. Res.*, **113**, D19306. https://doi.org/10.1029/2008JD009943.

——, ——, ——, M. Chong, and L. Descroix, 2010: Evolution of the stable water isotopic composition of the rain sampled along Sahelian Squall lines. *Quart. J. Roy. Meteor. Soc.*, **136**, 227–242, https://doi.org/10.1002/qj.485.

——, D. Noone, C. Frankenberg, and J. Worden, 2013: Role of continental recycling in intraseasonal variations of continental moisture as deduced from model simulations and water vapor isotopic measurements. *Water Resour. Res.*, **49**, 4136–4156, https://doi.org/10.1002/wrcr.20312.

Rozanski, K., L. Araguás-Araguás, and R. Gonfiantini, 1993: Isotopic patterns in modern global precipitation. *Climate Change in Continental Isotopic Records*, *Geophys. Monogr.*, Vol. 78, Amer. Geophys. Union, 1–36, https://doi.org/10.1029/GM078p0001.

Sachs, J. P., D. Sachse, R. H. Smittenberg, Z. Zhang, D. S. Battisti, and S. Golubic, 2009: Southward movement of the Pacific intertropical convergence zone AD 1400–1850. *Nat. Geosci.*, **2**, 519–525, https://doi.org/10.1038/ngeo554.

Sánchez-Murillo, R., A. M. Durán-Quesada, C. Birkel, G. Esquivel-Hernández, and J. Boll, 2017: Tropical precipitation anomalies and d-excess evolution during El Niño 2014–16. *Hydrol. Processes*, **31**, 956–967, https://doi.org/10.1002/hyp.11088.

Schmitt, S. R., D. A. Riveros-Iregui, and J. Hu, 2018: The role of fog, orography, and seasonality on precipitation in a semiarid, tropical island. *Hydrol. Processes*, **32**, 2792–2805, https://doi.org/10.1002/hyp.13228.

Scholl, M. A., and S. F. Murphy, 2014: Precipitation isotopes link regional climate patterns to water supply in a tropical mountain forest, eastern Puerto Rico. *Water Resour. Res.*, **50**, 4305–4322, https://doi.org/10.1002/2013WR014413.

——, S. E. Ingebritsen, C. J. Janik, and J. P. Kauahikaua, 1996: Use of precipitation and groundwater isotopes to interpret regional hydrology on a tropical volcanic island: Kilauea volcano area, Hawaii. *Water Resour. Res.*, **32**, 3525–3537, https://doi.org/10.1029/95WR02837.

——, S. B. Gingerich, and G. W. Tribble, 2002: The influence of microclimates and fog on stable isotope signatures used in interpretation of regional hydrology: East Maui, Hawaii. *J. Hydrol.*, **264**, 170–184, https://doi.org/10.1016/S0022-1694(02)00073-2.

——, T. W. Giambelluca, S. B. Gingerich, M. A. Nullet, and L. L. Loope, 2007: Cloud water in windward and leeward mountain forests: The stable isotope signature of orographic cloud water. *Water Resour. Res.*, **43**, W12411, https://doi.org/10.1029/2007WR006011.

——, J. B. Shanley, J. P. Zegarra, and T. B. Coplen, 2009: The stable isotope amount effect: New insights from NEXRAD echo tops, Luquillo Mountains, Puerto Rico. *Water Resour. Res.*, **45**, W12407, https://doi.org/10.1029/2008WR007515.

Shuler, C. K., H. Dulai, R. DeWees, M. Kirs, C. R. Glenn, and A. I. El-Kadi, 2019: Isotopes, microbes, and turbidity: A multi-tracer approach to understanding recharge dynamics and groundwater contamination in a basaltic island aquifer. *Ground Water Monit. Rem.*, **39**, 20–35, https://doi.org/10.1111/gwmr.12299.

Simpson, R. H., 1952: Evolution of the Kona storm a subtropical cyclone. *J. Atmos. Sci.*, **9**, 24–35, https://doi.org/10.1175/1520-0469(1952)009<0024:EOTKSA>2.0.CO;2.

Smith, R. B., 1989: Mountain-induced stagnation points in hydrostatic flow. *Tellus*, **41A**, 270–274, https://doi.org/10.1111/j.1600-0870.1989.tb00381.x.

——, 2019: 100 years of progress on mountain meteorology research. *A Century of Progress in Atmospheric and Related Sciences: Celebrating the American Meteorological Society Centennial*, *Meteor. Monogr.*, No. 59, Amer. Meteor. Soc., https://doi.org/10.1175/AMSMONOGRAPHS-D-18-0022.1.

——, and J. P. Evans, 2007: Orographic precipitation and water vapor fractionation over the Southern Andes. *J. Hydrometeor.*, **8**, 3–19, https://doi.org/10.1175/JHM555.1.

——, and Coauthors, 2012: Orographic precipitation in the tropics: The Dominica experiment. *Bull. Amer. Meteor. Soc.*, **93**, 1567–1579, https://doi.org/10.1175/BAMS-D-11-00194.1.

Sodemann, H., V. Masson-Delmotte, C. Schwierz, B. M. Vinther, and H. Wernli, 2008: Interannual variability of Greenland winter precipitation sources: 2. Effects of North Atlantic oscillation variability on stable isotopes in precipitation. *J. Geophys. Res.*, **113**, D12111, https://doi.org/10.1029/2007JD009416.

State of Hawaii, 2004: 2004 State of Hawaii Data Book. Dept. of Business, Economic Development and Tourism, 44 pp., https://files.hawaii.gov/dbedt/economic/databook/db2004/tableindex.pdf.

Stein, A. F., R. R. Draxler, G. D. Rolph, B. J. B. Stunder, M. D. Cohen, and F. Ngan, 2015: NOAA's HYSPLIT atmospheric transport and dispersion modeling system. *Bull. Amer. Meteor. Soc.*, **96**, 2059–2077, https://doi.org/10.1175/BAMS-D-14-00110.1.

Stewart, M. K., 1975: Stable isotope fractionation due to evaporation and isotopic exchange of falling waterdrops:

Applications to atmospheric processes and evaporation of lakes. *J. Geophys. Res.*, **80**, 1133–1146, https://doi.org/10.1029/JC080i009p01133.

Tachera, D. K., N. C. Lautze, G. Torri, and D. M. Thomas, 2021: Characterization of the isotopic composition and bulk ion deposition of precipitation from central to west Hawai'i island between 2017 and 2019. *J. Hydrol.*, **34**, 100786, https://doi.org/10.1016/j.ejrh.2021.100786.

Tierney, J. E., D. W. Oppo, Y. Rosenthal, J. M. Russell, and B. K. Linsley, 2010: Coordinated hydrological regimes in the Indo-Pacific region during the past two millennia. *Paleoceanogr. Paleoclimatol.*, **25**, PA1102, https://doi.org/10.1029/2009PA001871.

Tillman, F. D., D. S. Oki, A. G. Johnson, L. B. Barber, and K. R. Beisner, 2014: Investigation of geochemical indicators to evaluate the connection between inland and coastal groundwater systems near Kaloko-Honokōhau National Historical Park, Hawai'i. *Appl. Geochem.*, **51**, 278–292, https://doi.org/10.1016/j.apgeochem.2014.10.003.

Torri, G., D. Ma, and Z. Kuang, 2017: Stable water isotopes and large-scale vertical motions in the tropics. *J. Geophys. Res. Atmos.*, **122**, 3703–3717, https://doi.org/10.1002/2016JD026154.

Trenberth, K. E., 1997: The definition of El Niño. *Bull. Amer. Meteor. Soc.*, **78**, 2771–2778, https://doi.org/10.1175/1520-0477(1997)078<2771:TDOENO>2.0.CO;2.

Trujillo-Ortiz, A., 2022: gmregress, version 1.7.0.0. MathWorks, https://www.mathworks.com/matlabcentral/fileexchange/27918-gmregress.

Uemura, R., Y. Matsui, K. Yoshimura, H. Motoyama, and N. Yoshida, 2008: Evidence of deuterium excess in water vapor as an indicator of ocean surface conditions. *J. Geophys. Res.*, **113**, D19114, https://doi.org/10.1029/2008JD010209.

——, N. Yonezawa, K. Yoshimura, R. Asami, H. Kadena, K. Yamada, and N. Yoshida, 2012: Factors controlling isotopic composition of precipitation on Okinawa Island, Japan: Implications for paleoclimate reconstruction in the East Asian monsoon region. *J. Hydrol.*, **475**, 314–322, https://doi.org/10.1016/j.jhydrol.2012.10.014.

——, M. Uemura, M. Sano, and T. Nakatsuka, 2018: A 180-year-long isotopic record of tree-ring cellulose on Okinawa Island, Japan. *Geochem. J.*, **52**, e21–e27, https://doi.org/10.2343/geochemj.2.0543.

U.S. Census Bureau, 2020: Annual estimates of the resident population for the United States, regions, states, and the District of Columbia: April 1, 2010 to July 1, 2020, 2 pp., https://www.census.gov/programs-surveys/popest/technical-documentation/research/evaluation-estimates/2020-evaluation-estimates/2010s-state-total.html.

USGCRP, 2017: *Climate Science Special Report: Fourth National Climate Assessment, Volume I*. D. J. Wuebbles et al., Eds., U.S. Global Change Research Program, 470 pp., https://doi.org/10.7930/J0J964J6.

Veron, S., M. Mouchet, R. Govaerts, T. Haevermans, and R. Pellens, 2019: Vulnerability to climate change of islands worldwide and its impact on the tree of life. *Sci. Rep.*, **9**, 14471, https://doi.org/10.1038/s41598-019-51107-x.

Villiger, L., H. Wernli, M. Boettcher, M. Hagen, and F. Aemisegger, 2022: Lagrangian formation pathways of moist anomalies in the trade-wind region during the dry season: Two case studies from EUREC^{4}A. *Wea. Climate Dyn.*, **3**, 59–88, https://doi.org/10.5194/wcd-3-59-2022.

Vimeux, F., and C. Risi, 2021: Isotopic equilibrium between raindrops and water vapor during the onset and the termination of the 2005–2006 wet season in the Bolivian Andes. *J. Hydrol.*, **598**, 126472, https://doi.org/10.1016/j.jhydrol.2021.126472.

——, R. Gallaire, S. Bony, G. Hoffmann, and J. C. Chiang, 2005: What are the climate controls on δD in precipitation in the Zongo Valley (Bolivia)? Implications for the Illimani ice core interpretation. *Earth Planet. Sci. Lett.*, **240**, 205–220, https://doi.org/10.1016/j.epsl.2005.09.031.

——, P. Ginot, M. Schwikowski, M. Vuille, G. Hoffmann, L. G. Thompson, and U. Schotterer, 2009: Climate variability during the last 1000 years inferred from Andean ice cores: A review of methodology and recent results. *Palaeogeogr. Palaeoclimatol. Palaeoecol.*, **281**, 229–241, https://doi.org/10.1016/j.palaeo.2008.03.054.

Wang, Y. J., H. Cheng, R. L. Edwards, Z. S. An, J. Y. Wu, C.-C. Shen, and J. A. Dorale, 2001: A high-resolution absolute-dated Late Pleistocene monsoon record from Hulu Cave, China. *Science*, **294**, 2345–2348, https://doi.org/10.1126/science.1064618.

Weng, Y., A. Johannessen, and H. Sodemann, 2021: High-resolution stable isotope signature of a land-falling atmospheric river in southern Norway. *Wea. Climate Dyn.*, **2**, 713–737, https://doi.org/10.5194/wcd-2-713-2021.

Windhorst, D., T. Waltz, E. Timbe, H.-G. Frede, and L. Breuer, 2013: Impact of elevation and weather patterns on the isotopic composition of precipitation in a tropical montane rainforest. *Hydrol. Earth Syst. Sci.*, **17**, 409–419, https://doi.org/10.5194/hess-17-409-2013.

Yoshimura, K., and K. Ichiyanagi, 2009: A reconsideration of seasonal variation in precipitation deuterium excess over East Asia. *J. Japan Soc. Hydrol. Water Resour.*, **22**, 262–276.

——, M. Kanamitsu, and M. Dettinger, 2010: Regional downscaling for stable water isotopes: A case study of an atmospheric river event. *J. Geophys. Res.*, **115**, D18114, https://doi.org/10.1029/2010JD014032.

Zhang, Y., Y.-L. Chen, T. A. Schroeder, and K. Kodama, 2005: Numerical simulations of sea-breeze circulations over northwest Hawaii. *Wea. Forecasting*, **20**, 827–846, https://doi.org/10.1175/WAF859.1.

Zwart, C., N. C. Munksgaard, A. Protat, N. Kurita, D. Lambrinidis, and M. I. Bird, 2018: The isotopic signature of monsoon conditions, cloud modes, and rainfall type. *Hydrol. Processes*, **32**, 2296–2303, https://doi.org/10.1002/hyp.13140.